



**HAL**  
open science

## Two-photon absorption properties of multipolar triarylamino/tosylamido 1,1,4,4-tetracyanobutadienes

Nicolas Ripoche, Marie Betou, Clotilde Philippe, Yann Trolez, Olivier Mongin, Marta Dudek, Ziemowit Pokladek, Katarzyna Matczyszyn, Marek Samoc, Hiba Sahnoune, et al.

► **To cite this version:**

Nicolas Ripoche, Marie Betou, Clotilde Philippe, Yann Trolez, Olivier Mongin, et al.. Two-photon absorption properties of multipolar triarylamino/tosylamido 1,1,4,4-tetracyanobutadienes. *Physical Chemistry Chemical Physics*, 2021, 23 (39), pp.22283-22297. 10.1039/d1cp03346h . hal-03369351

**HAL Id: hal-03369351**

**<https://hal.science/hal-03369351>**

Submitted on 19 Oct 2021

**HAL** is a multi-disciplinary open access archive for the deposit and dissemination of scientific research documents, whether they are published or not. The documents may come from teaching and research institutions in France or abroad, or from public or private research centers.

L'archive ouverte pluridisciplinaire **HAL**, est destinée au dépôt et à la diffusion de documents scientifiques de niveau recherche, publiés ou non, émanant des établissements d'enseignement et de recherche français ou étrangers, des laboratoires publics ou privés.



Distributed under a Creative Commons Attribution - NonCommercial 4.0 International License

# Two-photon absorption properties of multipolar triarylamino/ tosylamido 1,1,4,4-tetracyanobutadienes

*Dedicated to the memory of Prof. François Diederich, an immense contributor to carbon chemistry*

Nicolas Ripoche,<sup>a,b</sup> Marie Betou,<sup>a</sup> Clotilde Philippe,<sup>a</sup> Yann Trolez,<sup>a,\*</sup> Olivier Mongin,<sup>a</sup> Marta Dudek,<sup>c</sup> Ziemowit Pokladek,<sup>c</sup> Katarzyna Matczyszyn,<sup>c,\*</sup> Marek Samoc,<sup>c</sup> Hiba Sahnoune,<sup>d,e</sup> Jean-François Halet,<sup>a,f,\*</sup> Thierry Roisnel,<sup>a</sup> Loïc Toupet,<sup>g</sup> Marie Cordier,<sup>a</sup> Graeme J. Moxey,<sup>b</sup> Mark G. Humphrey<sup>b,\*</sup> and Frédéric Paul<sup>a,\*</sup>

<sup>a</sup> Univ Rennes, CNRS, ENSCR, ISCR (Institut des Sciences Chimiques de Rennes) – UMR 6226, F-35000 Rennes, France.

<sup>b</sup> Research School of Chemistry, Australian National University, Canberra, ACT 2601, Australia

<sup>c</sup> Advanced Materials Engineering and Modelling Group, Faculty of Chemistry, Wrocław University of Science and Technology 50-370 Wrocław, Poland.

<sup>d</sup> Département de Chimie, Faculté des Sciences, Université M'Hamed Bouguara de Boumerdes, 35000, Boumerdes, Algeria.

<sup>e</sup> Laboratoire de Physique et Chimie Quantique, Université Mouloud Mammeri de Tizi Ouzou, 15000, Tizi Ouzou, Algeria.

<sup>f</sup> CNRS–Saint-Gobain–NIMS, IRL 3629, Laboratory for Innovative Key Materials and Structures (LINK), National Institute for Materials Science (NIMS), Tsukuba, 305-0044, Japan.

<sup>g</sup> Univ Rennes, CNRS, Institut de Physique de Rennes (IPR) – UMR 6251, F-35000 Rennes, France.

*The synthesis and characterization of four new tetracyanobutadiene (TCBD) derivatives (1, 3c and 4b-c) incorporating tosylamido and 4-triphenylamino moieties are reported. Along with those of five closely related or differently branched TCBDs derivatives (2, 3a-b, 4c and 5), their linear and (third-order) nonlinear optical properties were investigated by electronic absorption spectroscopy and Z-scan measurements. Among these compounds, the tri-branched compounds 3c and 5 are the most active two-photon absorbers, with effective cross-sections of 275 and 350 GM at 900 nm, respectively. These properties are briefly discussed with the help of DFT calculations, focussing on structural and electronic factors, and contextualized with results obtained previously for related compounds.*

## Introduction

Tetracyanobutadienes (TCBDs) are powerful electron-accepting groups<sup>1-12</sup> that give rise to electrochromic dipolar or multipolar structures,<sup>13, 14</sup> often possessing remarkable cubic nonlinear optical (NLO) properties and high thermal stability.<sup>15-20</sup> Their synthesis usually involves tetracyanoethylene (TCNE) and an electron-rich alkyne, thus leading to a [2+2] cycloaddition-retroelectrocyclization (CA-RE) sequence.<sup>14, 21</sup> The yield of the reaction depends on the nature of the moiety that enriches the C≡C bond of the precursor. This enriching moiety not only impacts the yield but also affects the optical properties of the TCBDs, both in absorption and in emission. For example, while TCBDs are generally described as non-emissive,<sup>22, 23</sup> recent papers reported fluorescent TCBDs effective in different wavelength range.<sup>24-29</sup> In linear absorption, the lowest energy band is usually dominated by an intramolecular charge transfer from the initially enriching moiety and the TCBD core, except in the case of TCBD derived from ynamides where the situation differs significantly.<sup>1, 30, 31</sup> This situation motivated us to investigate nonlinear absorption properties of a variety of TCBDs synthesized from differently-enriched alkynes (anilines, ferrocenes and ynamides). We anticipated different properties given the nature of the enriching moiety and the number of TCBD groups in each molecule.

Because TCBD derivatives such as **A<sub>x</sub>** (Chart 1) possess sizeable two-photon absorption (2PA) cross-sections in the near-IR region (800-1050 nm),<sup>24</sup> a wavelength range of interest for various innovative applications (optical limiting, data storage, nanofabrication, etc),<sup>32-34</sup> we were interested in measuring the 2PA properties of linear analogues such as **1-3a** and of branched derivatives such as **3b-c**. While assessing the 2PA cross-sections ( $\sigma_2$ ) of these simple multipolar TCBD derivatives, we also wanted to investigate the effect of branching at the triarylamino core.<sup>35</sup> The **4a-c** series was therefore targeted as model compounds to better delineate the role of symmetry (dipolar/linear vs. octupolar/branched) on their 2PA properties. Finally, given that functionalization by transition metal complexes is a well-known way to boost the third-order NLO properties,<sup>36,37-39</sup> we were interested in comparing the 2PA properties of the triphenylamino-based derivatives **3c** and **4c** with those of their known metallated analogue **5**.<sup>13</sup>

We report, herein, the synthesis of four new derivatives required for this study, their 1PA and 2PA properties, assignment of the former from time-dependent density functional theory (TD-DFT) calculations, and comparison with relevant literature data for related derivatives.

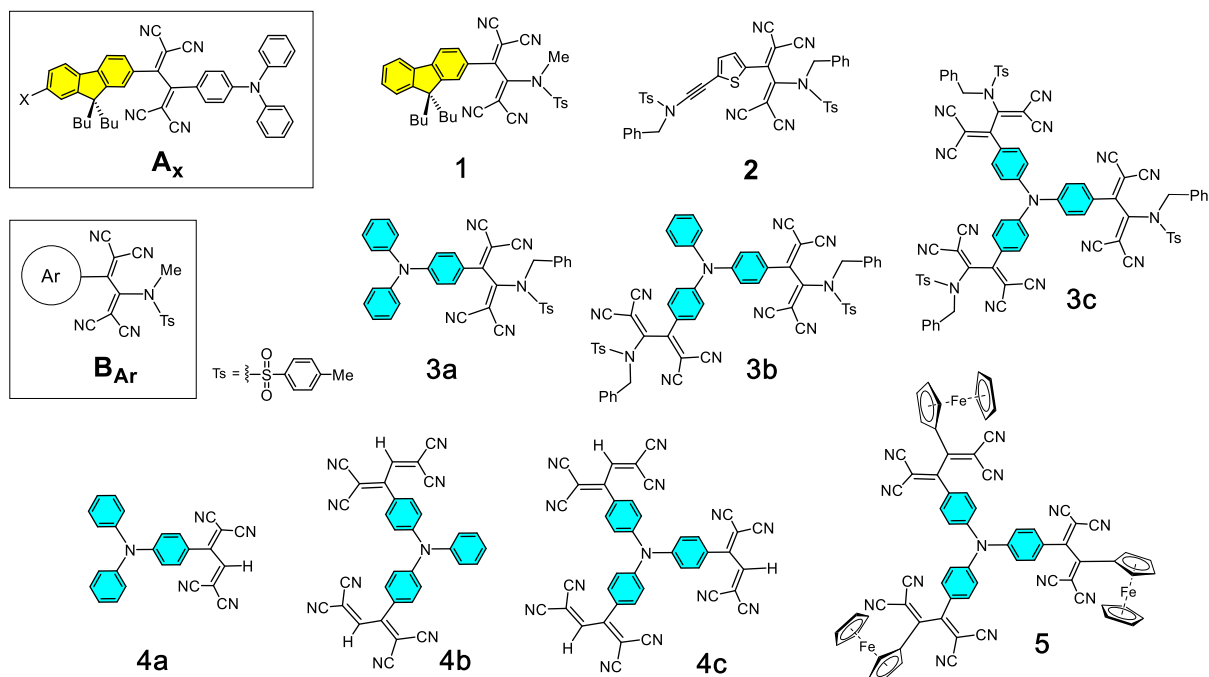
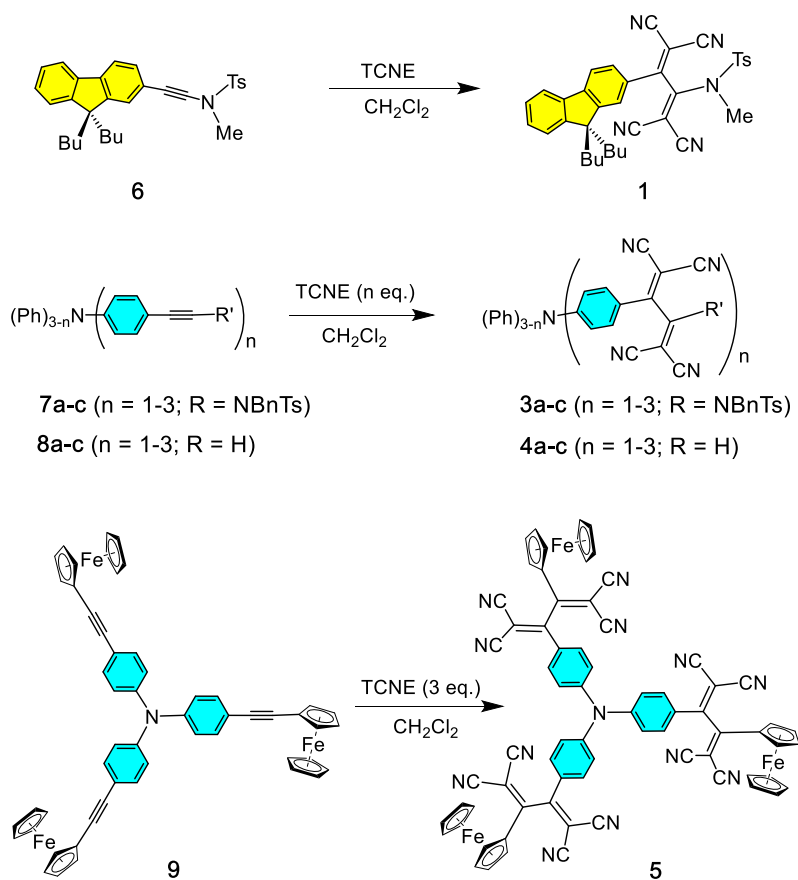


Chart 1. Molecules targeted in this work and (inset) previously isolated TCBD derivatives **A<sub>x</sub>**<sup>24</sup> and **B<sub>Ar</sub>**.<sup>30</sup>

## Results

### Synthesis of the TCBD compounds



Scheme 1. Synthesis of **1**, **3a-c**, **4a-c** and **5**.



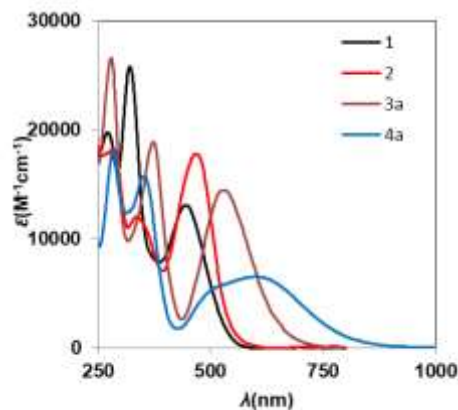


Figure 2. UV-Vis spectra of mono-TCBD compounds **1-4a** in CH<sub>2</sub>Cl<sub>2</sub> at 25 °C.

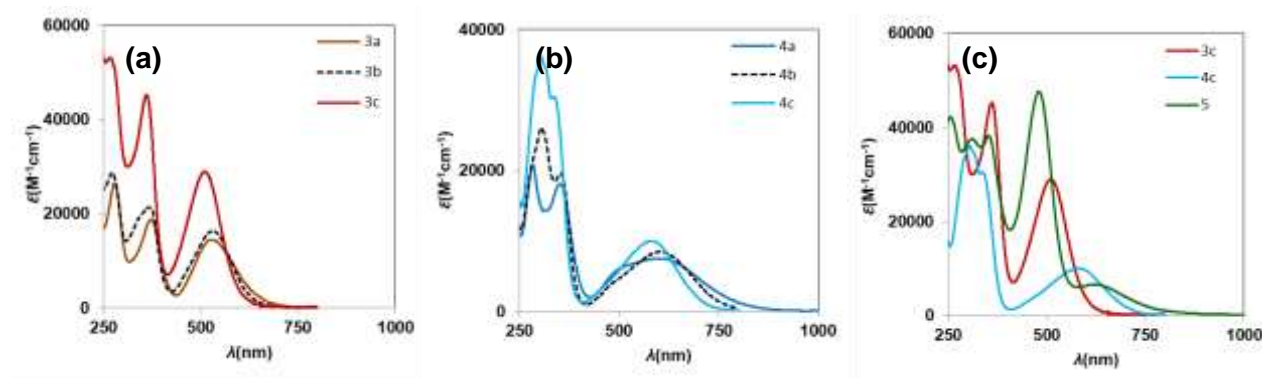
### Linear Optical Properties

Table 1. Selected 1PA and Electrochemical Data in CH <sub>2</sub> Cl <sub>2</sub> <sup>[a]</sup> for <b>1-5</b> and <b>A<sub>H</sub></b> .				
Cmpd	Main Absorption(s) λ (nm) <sup>a</sup> [ε (10 <sup>3</sup> M <sup>-1</sup> ·cm <sup>-1</sup> )]	E <sup>o</sup> <sup>b</sup> 1 <sup>st</sup> red. (TCBD)	E <sup>o</sup> <sup>b</sup> 1 <sup>st</sup> oxid. (donor)	λ <sup>51</sup> <sup>c</sup> [ΔG <sub>CS</sub> ] (eV)
<b>1</b>	272 [19.7], 321 [25.8], 445 [13.1]	/	/	/
<b>2</b>	285 [18.2], 337 [12.0], 468 [17.8]	-0.52 <sup>d</sup> -0.91 <sup>d</sup>	/	/
<b>3a</b>	279 [32.0], 373[22.7], 531 [17.4]	-0.60 <sup>e</sup> -1.01 <sup>e</sup>	0.72 <sup>e,f</sup>	2.33 [0.98]
<b>3b</b>	272 [28.6], 369 [21.3], 533 [16.3]	-0.52 <sup>[d]</sup> -0.63 <sup>[d]</sup> -1.04 <sup>[d]</sup>	/	/
<b>3c</b>	268 [53.2], 361 [45.3], 508 [29.0]	/	/	/
<b>4a</b>	286 [17.7], 354 [15.7], 545 [sh, 5.8], 602 [6.5]	-0.62 <sup>g</sup> -1.27 <sup>g</sup>	0.85 <sup>f,g</sup>	2.06 [1.20]
<b>4b</b>	306 [26.2], 354 [19.6], 505 [sh, 4.9], 604 [8.4]	/	/	/
<b>4c</b>	305 [36.1], 338 [30.4], 495 [sh, 5.5], 581 [10.0]	/	/	/
<b>5</b>	257 [42.2], 311 [35.5], 353 [38.2], 481 [47.6], 624 [6.6]	-0.95 <sup>h</sup> -1.07 <sup>h</sup> -1.33 <sup>h</sup>	0.41 <sup>f,h</sup>	1.98 [0.91]
<b>A<sub>H</sub></b>	274 [24.9], 340 [15.9], 414 [33.9], 489 [25.3]	-0.41 <sup>d</sup> -0.77 <sup>d</sup>	1.31 <sup>d</sup>	2.54 [1.46]

<sup>a</sup> Unless otherwise stated. <sup>b</sup> Oxidation potential vs. FcH<sup>+</sup>/FcH in V (± 5 mV). <sup>c</sup> Energy (eV) of the first allowed absorption [Energy (eV) of the lowest-lying charge separated (CS) state derived from Rehm-Weller eqns (ESI)].<sup>24</sup> <sup>d</sup> In CH<sub>2</sub>Cl<sub>2</sub>/[<sup>n</sup>Bu<sub>4</sub>N][PF<sub>6</sub>] (0.1M).<sup>30</sup> <sup>e</sup> In CH<sub>3</sub>CN/[<sup>n</sup>Bu<sub>4</sub>N][PF<sub>6</sub>] (0.1 M).<sup>1</sup> <sup>f</sup> Chemically not reversible. <sup>g</sup> In CH<sub>2</sub>Cl<sub>2</sub>/[<sup>n</sup>Bu<sub>4</sub>N][PF<sub>6</sub>] (0.1 M).<sup>7</sup> <sup>h</sup> This work: in CH<sub>2</sub>Cl<sub>2</sub>/[NBu<sub>4</sub>][PF<sub>6</sub>] (0.1 M).

The derivatives **1-5** exhibit a strong absorption band in the visible range extending, in the case of **3-5**, beyond 700 nm (Figure 2 and Table 1). Except for **4a**, this band corresponds to several (overlapping) charge-transfer (CT) transitions (see DFT section). Its strong  $\pi$ - $\pi^*$  character is supported by its weak solvatochromism (see ESI for selected spectra in CH<sub>2</sub>Cl<sub>2</sub> and THF; Figure S10).<sup>1,24</sup> More precisely, for compounds **1** and **2**, which lack a strongly electron-releasing group on the TCBD unit, the absorption band at lowest energy (Figure 2) originates from overlapping charge-transfer (CT) transitions from the aromatic fragments (2-fluorenyl or 2-thienyl) and from the tosylamido group (and also

from the substituent appended to its nitrogen atom) toward the dicyanovinyl groups of the TCBD unit.<sup>1</sup> Upon proceeding to compounds with more electron-rich aromatic groups (*i.e.* 4-*N,N*-diphenylanilino), the “Ar $\rightarrow$ =C(CN)<sub>2</sub>” transition shifts to lower energy and eventually deconvolutes from the other band. This results in an overall bathochromic shift and splitting of this first absorption band upon increasing the electron-richness of the aromatic group from **1** to **2**, and further to **3a** and **4a**. For the tosylamido derivatives in **1-3a**, another intense band incorporating a second “N(R)Tos $\rightarrow$ =C(CN)<sub>2</sub>” CT transition (R= Me, Bz) is expected at higher energy (around 320-350 nm),<sup>1</sup> while for the two diphenylanilino derivatives **3-4a**, the absorption bands around 280-320 nm likely contain contributions of characteristic triaryl-amino-centered  $\pi\rightarrow\pi^*$  transitions.<sup>45</sup> For these two derivatives, it is thus predominantly the presence of the 4-diphenylanilino group which determines the energy and intensity of the first absorption band. The presence of a weakly electron-donating tosylamido group in **3a** limits somewhat the electron-accepting capability of the TCBD moiety compared to **4a**. As a result, this first CT transition is less red-shifted in **3a** (Figure 2).



**Figure 3.** UV-Vis spectra of triaryl-amino derivatives **3a-c** (a), **4a-c** (b) and the tri-branched derivatives **3a**, **4a** and **5** (c) in CH<sub>2</sub>Cl<sub>2</sub> at 25 °C.

The effect of branching at the triphenylamino core can then be assessed by considering the families **3a-c** and **4a-c** (Figures 3a-b). Proceeding from **3a/4a** to the corresponding tri-branched derivatives **3c/4c** results in a slight blue shift and an increase in intensity of the first absorption band in both cases. Although such blue-shifts upon branching are uncommon for related triphenylamine families,<sup>46, 47</sup> they were predicted in the present case based on DFT computations. In the case of the tris-ferrocenyl compound **5** (Figure 3c), a moderate-to-weak transition is observed near 650 nm and a second more intense band around 480 nm. The former corresponds to a CT transition, from the ferrocenyl fragment toward the TCBD moiety (see DFT section),<sup>13a</sup> while the latter corresponds to the amino-to-TCBD CT observed at lowest energy for the organic derivatives **3c** and **4c** (Figure 3c). When progressing from **3c** to **4c** and **5**, the first band experiences a red shift which reflects the substitution of the TCNE moiety by more and more electron-releasing substituents (Fc > N(Bz)Ts > H). The third band of **5** is likely similar to the third one in **3c** and corresponds to a  $\pi\rightarrow\pi^*$  transition characteristic of the triphenylamine core,<sup>44</sup> while that near 260 nm possibly corresponds to another ferrocene-based MLCT transition.<sup>48</sup>

### Z-scan Studies

In line with previous findings for **A<sub>x</sub>** derivatives (X = H, NPh<sub>2</sub>),<sup>24</sup> all TCBD derivatives **1-5** were essentially non-emissive in solution at 25 °C and poorly emissive in solvent glasses at low temperature. To measure their 2PA properties, we therefore had to resort to the Z-scan technique to determine their effective 2PA cross-sections ( $\sigma_{\text{eff}}$ ).<sup>49</sup> Under the conditions used, positive  $\sigma_{\text{eff}}$  values should correspond to  $\sigma_2$  values provided that no excited-state absorption (ESA) occurs.<sup>50, b</sup> For all compounds, the Z-scan spectra were recorded in THF to minimize any unwanted photoinduced electron-transfer to the solvent, except for **4a** which slowly reacted in that solvent (even in the dark). Thus, CH<sub>2</sub>Cl<sub>2</sub> was eventually used for performing the Z-scan measurements with this particular compound (Table 2). Considering the weak 1PA solvatochromism observed between THF and CH<sub>2</sub>Cl<sub>2</sub> for **3a-c**, the spectra in either of these solvents should be suitable for comparison between the 1PA and 2PA spectra of the tosylamido derivatives (**1-3c**).

**Closed-aperture Z-scan measurements.** The molecular third-order NLO coefficients of these compounds are dominated by their real parts ( $\gamma_{\text{Re}}$ ), in line with previous results obtained with **A<sub>x</sub>** derivatives (ESI, Figures S21-S22).<sup>24</sup> Except for **5**, these are usually

<sup>a</sup> The fact that the energy of the lowest-energy CT bands is always greater than the enthalpy of formation of the donor<sup>+</sup>/TCBD<sup>-</sup> charge separated state ( $\Delta G_{\text{CT}}$  in Table 1), as evaluated from CV data gathered in the same solvent, reveals the existence of a sizeable reorganization energy in this first singlet excited state (of ca. 1.0-1.2 eV).<sup>29</sup>

<sup>b</sup> Reverse saturable absorption (RSA) can be excluded because the 2PA bands do not overlap with the one-photon absorption (1PA) bands.

negative with large peaks being observed in the near-IR domain (800-1700 nm). However, the large experimental uncertainties preclude the accurate evaluation of  $\gamma_{\text{Re}}$  values for many of these compounds.

**Open-aperture Z-scan measurements.** In contrast, the determination of the maximal values of their nonlinear absorption parameters was always more precise. For each compound, many of the detected 2PA peaks overlap with peaks on the 1PA spectrum plotted against twice the wavelength (Figures 4, 8, 9, S23 and S24). This allows identification of the 1PA excited states populated by two-photon absorption. In the case of **3a-c** and **5**, two 2PA maxima instead of one were detected, suggesting that different excited states composing the 1PA band are populated by two-photon excitation. We will return to these observations in the Discussion section.

**Table 2.** 2PA Data for **1-5** and **A<sub>H</sub>** and **A<sub>NPh2</sub>** determined by Z-scan in THF.

Cmpd	$\lambda_{1\text{PA}}^a$ (nm)	$\lambda_{2\text{PA}}^b$ (nm)	$\sigma_{2\text{max}}^c$ (GM)	$\sigma_{2\text{max}}/N_{\text{eff}}^{2d}$ (GM)	$\sigma_{2\text{max}}/MW^e$ (GM/g)
<b>1</b>	445 <sup>f</sup>	875	55 ± 10	0.13	0.09
<b>2</b>	468 <sup>f</sup>	900 <sup>f</sup>	120 ± 10	0.35	0.15
<b>3a</b>	518	1100 900	55 ± 7 50 ± 4	0.15 0.16	0.08 0.08
<b>3b</b>	524	1150 1050 950	90 ± 15 175 ± 15 170 ± 20	0.15 0.30 0.29	0.08 0.16 0.16
<b>3c</b>	509	1150 900	80 ± 30 275 ± 20	0.10 0.34	0.19 0.05
<b>4a</b>	602 <sup>f</sup>	1300 <sup>f</sup>	30 ± 2 <sup>f</sup>	0.11 <sup>f</sup>	0.08 <sup>f</sup>
<b>4b</b>	552	1150	75 ± 5	0.14	0.14
<b>4c</b>	528	1150	100 ± 5	0.17	0.14
<b>5</b>	475 608	1300 1150 980 900	25 ± 5 90 ± 5 225 ± 90 ≥350 ± 90	0.02 0.09 0.22 0.34	0.02 0.07 0.18 0.28
<b>A<sub>H</sub></b>	489 <sup>f</sup>	925	115 ± 10	0.21	0.17
<b>A<sub>NPh2</sub></b>	512 <sup>f</sup>	1050	390 ± 50	0.62	0.46

<sup>a</sup> Wavelength of the lowest energy 1PA maximum. <sup>b</sup> Wavelength of the maximal 2PA value detected. <sup>c</sup> Cross-section at maximum. <sup>d</sup>  $N_{\text{eff}}$  is the effective number of  $\pi$  electrons in a conjugated system (see ESI).<sup>51</sup> <sup>e</sup> Figure of merit relevant for applications in optical limiting or nanofabrication.<sup>34</sup> In this expression,  $MW$  represents the molecular weight. <sup>f</sup> Measured in  $\text{CH}_2\text{Cl}_2$ .

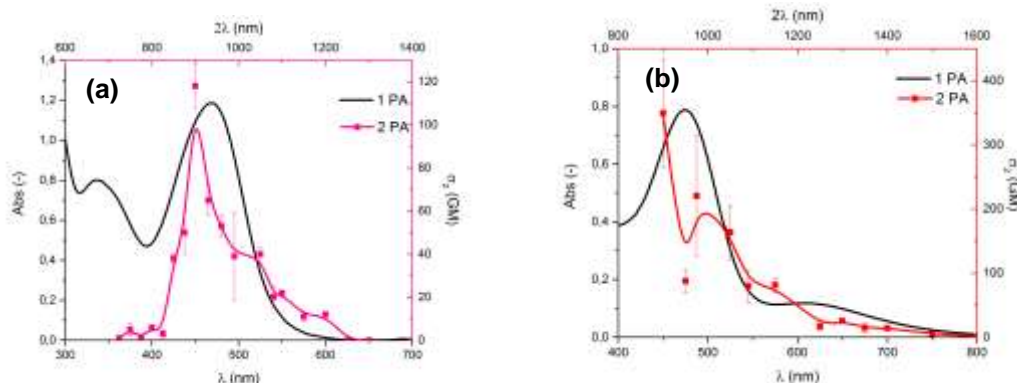


**Figure 4.** Overlay of one and two-photon absorption spectra for **2** (a) and **5** (b) in THF at 25 °C. The 2PA cross-sections are derived from open-aperture Z-scan measurements and the 1PA spectra are plotted against twice the wavelength ( $2\lambda$ ).

Finally, to consistently compare the NLO responses obtained for different compounds, some normalization procedure should be used to identify the “best” two-photon absorbers suited to a given application. One possibility is to correct for the molecular weight  $MW$  (also correlated to the “size” of the molecule),<sup>34</sup> while another is to correct for the so-called “effective” number of  $\pi$  electrons ( $N_{eff}$ ), following a concept developed by Kuzyk (ESI, Table S2).<sup>51, 52</sup> According to both criteria, all the new organic derivatives are less active than the  $A_{NPh_2}$  derivative previously investigated.<sup>24</sup> Based on these figures of merit, the organometallic derivative **5** has larger figures of merit, demonstrating the positive impact of the organometallic substituents on the third-order NLO properties within this class of compounds.

## DFT Calculations

Density functional theory (DFT) calculations were carried out on these different compounds to better understand their electronic structures and linear absorptions. Real structures **2-5** were used for calculations, except for **1** for which a simplified model (**1'**) in which the butyl chains were replaced by methyl groups was used to expedite the calculations. In addition, **6** (see Chart 2), representing a single branch of **5**, was also computed for comparison purpose. To facilitate assignment of the UV-Vis absorption spectra for **1-5**, time-dependent (TD)-DFT calculations were then performed on **1'-6**, but the modelling of long-range charge transfer transitions proved problematic.<sup>53</sup> The energies of the various transitions were highly sensitive to the functional used, but less so to the surrounding dielectric medium, a slight red-shift of the first absorption (compared to experiment) always being computed when the solvent (THF or  $CH_2Cl_2$ ) was taken into consideration (PCM model). As a result, all optimizations and calculations were carried out in vacuum using the mPW1PW91 functional, a combination which gave the best match with experimental data for the organic derivatives.<sup>54, 55</sup> In addition, for purpose of comparison,  $A_H$ <sup>24</sup> was also recomputed using the same functional. Only for the two organometallic models (**5** and **6**), which have more polarizable  $d$  orbitals, was the THF solvent considered in the calculations (*via* PCM).

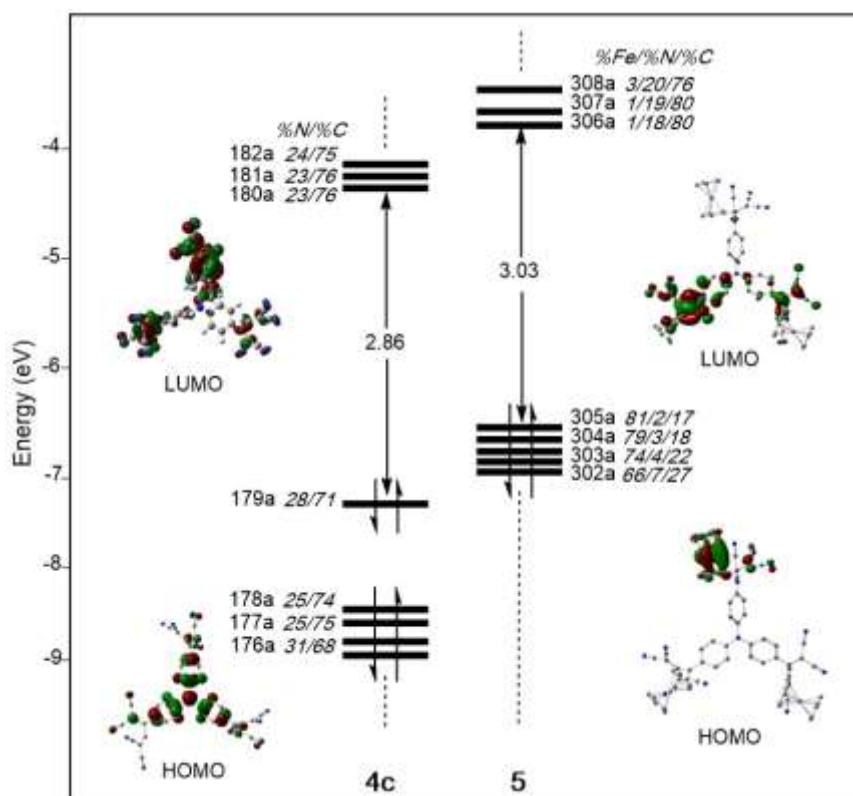
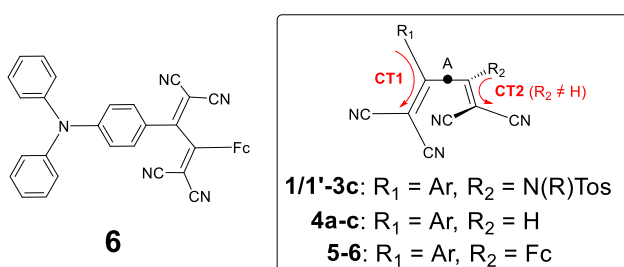


**Figure 5.** Comparison of the FMO diagrams of **4c** (left) and **5** (right). Atomic percentage contributions of the FMOs are given in italics.





A glance at the nodal properties of the frontier molecular orbitals (MOs) of the different TCBD organic derivatives indicates that the highest occupied molecular orbital (HOMO) is mostly localized on the aromatic fragment (fluorenyl or thienyl) for the organic derivatives **1'** and **2**, or on the triphenylamino fragment for **3a-c** and **4a-c** (Figure S12, ESI). The lowest unoccupied molecular orbitals (LUMO) and LUMO+1 are always strongly localized on the TCBD fragment(s) for all compounds. In line with the available CV data (Table 1 and ESI, Figure S7), this confirms that oxidation will mostly affect the donor group (aromatic rings in **1'** and **2**, triphenylamine in **3a-c**, **4a-c**), whereas reduction will lead to injection of an electron into the  $\pi$  manifold of the TCBD units.

**Table 3.** Calculated dipole moments and HOMO-LUMO gaps for **1'-5** and **A<sub>H</sub>**.

Cmpd	$\mu$ [D] <sup>a</sup>	HOMO-LUMO gap [eV]
<b>1'</b>	7.89	2.88
<b>2</b>	12.08	2.93
<b>3a</b>	10.28	2.63
<b>3b</b>	17.27	2.57
<b>3c</b>	24.96	2.66
<b>4a</b>	12.41	2.59
<b>4b</b>	11.05	2.66
<b>4c</b>	6.50	2.86
<b>5</b>	9.84	3.03
<b>6</b>	12.29	3.35
<b>A<sub>H</sub></b>	9.41	2.77

<sup>a</sup> For compounds **3c**, **4c** and **5**, the main component of the dipole moment is perpendicular to the mean molecular plane of the octupolar triarylamine core (ESI).

A closer look at the dipole moments computed for these compounds (Table 3 and Figures S13-S14) reveals that among the mono-TCBD derivatives, only **4a** can be considered as a dipolar compound with its dipole moment roughly oriented along the Ph<sub>2</sub>N-TCBD axis. For compounds **1'-2**, **3a** and even **6**, due to the nonplanar conformation adopted by the TCBD moiety (Chart 2), the main component of the dipole moment remains roughly in the mean plane defined by the TCBD axis and the two connecting atoms of R<sub>1</sub> and R<sub>2</sub>, but usually bisects the R<sub>1</sub>-A-R<sub>2</sub> angle, both R<sub>1</sub> and R<sub>2</sub> acting as potential electron-releasing groups. This geometrical conformation has to be kept in mind when considering the TD-DFT computations. Thus, among the tri-branched derivatives **3c**, **4c** and **5**, only **4c** might be considered as an octupolar compound, the two others having higher multipolarity. These calculations indicate also that replacing the hydrogen substituent(s) at R<sub>2</sub> in **4a-c** by more electron-releasing substituents contributes to an increase in the HOMO-LUMO gap, and therefore contributes to stabilizing the compounds electronically (in addition to reinforcing the steric shielding of the TCBD unit).

For the organic derivatives, gas-phase TD-DFT calculations reproduced the experimentally observed spectra within a maximum error of *ca.* 3500 cm<sup>-1</sup>/0.43 eV (Table 4). The first allowed (singlet-singlet) excitation involves in all cases the HOMO→LUMO transition with a strong CT character in **1'-4c**, followed by other CT transitions at higher energies, as previously found for **A<sub>x</sub>** derivatives.<sup>24</sup> Among the mono-TCBD derivatives **1'-2**, **3a** and **4a** (Chart 2), the latter (with R<sub>2</sub> = H) constitutes the simplest case; its first absorption band corresponds to a single donor-acceptor (Ph<sub>2</sub>N → TCBD) transition. For the other derivatives, which possess another electron-releasing substituent at R<sub>2</sub>, two CT excited states can be accessed upon excitation. In line with previous findings,<sup>1</sup> when an aromatic group is appended at R<sub>1</sub> (2-thienyl, 2-fluorenyl) and a tosylamido group at R<sub>2</sub>, these two CT transitions partially merge, giving rise to two distinct excitations that overlap to give single absorption bands at lowest energy. The band at next-higher energy similarly corresponds to more than one underlying CT transition. Only in the case of the most electron-rich aromatic group (4-diphenylanilino), *i.e.* **3a**, does a single CT transition dominate the first band (CT1; see Chart 2), the CT transition originating from the tosylamido group (CT2) contributing to the band at next-higher energy. However, even in this case, calculations indicate that two distinct and overlapping transitions still contribute to the first absorption band. Finally, for all compounds, the absorption bands at wavelengths below 350 nm involve  $\pi \rightarrow \pi^*$  transitions largely localized on the aromatic fragment.

The influence of branching is exemplified by the series of compounds **4a-c**. Upon progressing from **4a** to **4c**, the arm-centered CT transitions become degenerate and combine on symmetry grounds,<sup>56</sup> giving rise to two (one-photon) allowed transitions in the case of **4b** (of *B* and *A* symmetry) and also to two transitions in the case of **4c** (of *A* and *E* symmetry), for which only the  $E \leftarrow A$

transition is fully (one-photon) allowed in the latter case. These sets of transitions can be easily identified (Table 1), even when no symmetry is imposed. The corresponding excited states have been labelled in Figure 6. Their energetic splitting<sup>46</sup> depends on the electronic (excitonic) coupling  $V$  between the arm-centered transitions ( $2V = 0.11$  eV and  $3V = 0.11$  eV for **4b** and **4c**, respectively), and this is weak; as a result, the electronic spectra of **4b** and **4c** are qualitatively very similar to that of **4a**, except for their intensity.<sup>47</sup> The same situation exists for the series **3a-c** (Figure 6), except that several arm-centered transitions are involved in the first absorption band, each of which is split by roughly the same energy upon branching in **3b-c** (e.g.  $3V$  corresponding to *ca.* 0.15-0.20 eV in **3c**). As a result, the first absorption band is also broadened.

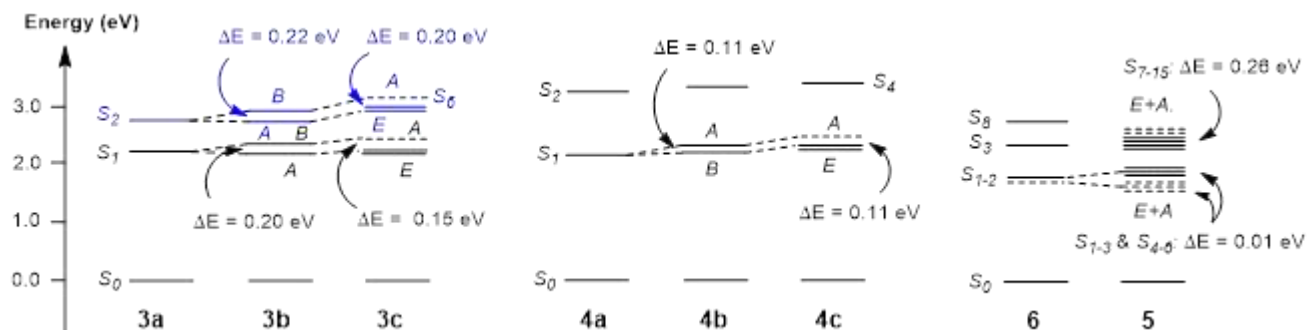


**Figure 6.** First singlet excited states computed for **3a-c**, **4a-c**, **5** and **6**. Dotted lines represent “forbidden” 1PA states ( $f < 0.02$ ).

**Table 4.** Experimental ( $\text{CH}_2\text{Cl}_2$ ) vs. computed <sup>a</sup> (mPW1PW91/LANL2DZ) values in vacuum. Wavelength (nm) and composition of the first relevant singlet excited states (wavelength [oscillator strength], transition percentage, assignment).

Cmpd	Experimental	Calculated <sup>c</sup>	Composition	Major Assignment <sup>e</sup>
	$\lambda_{\text{max}}$ [ $\epsilon$ ] <sup>b</sup>	$\lambda_{\text{max}}$ [ $f$ ] <sup>d</sup>		
<b>1'</b>	445 [13.1]	527 [0.18]	133→134 (98%)	$(\pi^*)_{\text{TCBD}} \leftarrow (\pi)_{\text{Fluo}}$
		373 [0.13]	130→134 (52%) 133→135 (23%)	$(\pi^*)_{\text{TCBD/Ts}} \leftarrow (\pi)_{\text{Ts/Fluo}}$
	321 [25.8]	364 [0.24]	133→135 (67%)	$(\pi^*)_{\text{TCBD/Ts}} \leftarrow (\pi)_{\text{Fluo}}$
		329 [0.08]	129→134 (82%)	$(\pi^*)_{\text{TCBD}} \leftarrow (\pi)_{\text{Fluo}}$
	272 [19.7]	309 [0.10]	131→135 (44%) 130→135 (35%)	$(\pi^*)_{\text{TCBD/Ts}} \leftarrow (\pi)_{\text{Fluo}}$
		297 [0.26]	133→136 (74%)	$(\pi^*)_{\text{Ts/TCBD}} \leftarrow (\pi)_{\text{Fluo}}$
<b>2</b>	468 [17.8]	534 [0.18]	187→188 (90%)	$(\pi^*)_{\text{TCBD}} \leftarrow (\pi)_{\text{Thio}}$
		405 [0.09]	185→188 (72%)	$(\pi^*)_{\text{TCBD}} \leftarrow (\pi)_{\text{Bz1}}$
	337 [12.0]	401 [0.26]	186→188 (50%) 185→188 (20%) 185→188 (20%)	$(\pi^*)_{\text{TCBD/Ts}} \leftarrow (\pi)_{\text{Thio/Bz1-2}}$
		344 [0.6]	185→189 (70%)	$(\pi^*)_{\text{TCBD/Ts}} \leftarrow (\pi)_{\text{Bz1}}$
	285 [18.2]	326 [0.14]	187→191 (66%)	$(\pi^*)_{\text{2Ts/TCBD/CC}} \leftarrow (\pi)_{\text{Thio}}$
<b>3a</b>	531 [17.4]	582 [0.15]	166→167 (98%)	$(\pi^*)_{\text{TCBD}} \leftarrow (\pi)_{\text{PhNPh2}}$
		459 [0.23]	166→168 (98%)	$(\pi^*)_{\text{TCBD/Ts}} \leftarrow (\pi)_{\text{PhNPh2}}$
	373[22.7]	367 [0.09]	165→167 (81%)	$(\pi^*)_{\text{TCBD}} \leftarrow (\pi)_{\text{PhNPh2/Bz}}$
		360 [0.15]	166→169 (75%)	$(\pi^*)_{\text{TCBD/Ts}} \leftarrow (\pi)_{\text{PhNPh2}}$
	279 [32.0]	288 [0.15]	166→173 (78%)	$(\pi^*)_{\text{NPh3}} \leftarrow (\pi)_{\text{PhNPh2}}$

<sup>c</sup> If the high-energy shoulder on the first absorption band of **4b** and **4c** corresponds to the additional band resulting from this coupling, a larger coupling than presently computed would be effective in the real molecules.

<b>3b</b>	533 [16.3]	598 [0.24]	267→268 (98%)	<b>A:</b> $(\pi^*)_{\text{TCBD}} \leftarrow (\pi)_{\text{PhNPh}_2}$
		544 [0.14]	267→269 (98%)	<b>B:</b> $(\pi^*)_{\text{TCBD}} \leftarrow (\pi)_{\text{PhNPh}_2}$
		456 [0.22]	267→270 (98%)	<b>A:</b> $(\pi^*)_{\text{TCBD/Ts}} \leftarrow (\pi)_{\text{PhNPh}_2}$
		422 [0.12]	267→271 (98%)	<b>B:</b> $(\pi^*)_{\text{TCBD/Ts}} \leftarrow (\pi)_{\text{PhNPh}_2}$
	369 [21.3]	375 [0.09]	264→268 (56%)	$(\pi^*)_{\text{TCBD}} \leftarrow (\pi)_{\text{PhNPh}_2/\text{Bz}}$
	351 [0.15]	267→272 (38%) 265→268 (16%) 261→268 (14%)	$(\pi^*)_{\text{TCBD/Ts}} \leftarrow (\pi)_{\text{PhNPh}_2/\text{Bz}}$	
<b>3c</b>	508 [29.0]	574 [0.27]	368→369 (98%) 368→370 (98%)	<b>E:</b> $(\pi^*)_{\text{TCBD}} \leftarrow (\pi)_{\text{NPh}_3}$
		537 [0.004]	368→371 (98%)	<b>A:</b> $(\pi^*)_{\text{TCBD}} \leftarrow (\pi)_{\text{NPh}_3}$
		437 [0.22]	368→372 (98%) 368→373 (98%)	<b>E:</b> $(\pi^*)_{\text{TCBD/Ts}} \leftarrow (\pi)_{\text{NPh}_3}$
		408 [0.0004]	368→374 (95%)	<b>A:</b> $(\pi^*)_{\text{TCBD/Ts}} \leftarrow (\pi)_{\text{NPh}_3}$
	361 [45.3]	384 [0.07]	365→369 (31%) 366→369 (17%) 367→370 (17%)	$(\pi^*)_{\text{TCBD}} \leftarrow (\pi)_{\text{Bz}}$
<b>4a</b>	602 [6.5]	592 [0.18]	103→104 (98%)	$(\pi^*)_{\text{TCBD}} \leftarrow (\pi)_{\text{PhNPh}_2}$
	354 [15.7]	387 [0.49]	103→105 (90%)	$(\pi^*)_{\text{TCBD/PhN}} \leftarrow (\pi)_{\text{PhNPh}_2}$
		354 [0.14]	102→104 (86%)	$(\pi^*)_{\text{TCBD/Ph}} \leftarrow (\pi)_{\text{PhNPh}_2/\text{TCBD}}$
	286 [17.7]	288 [0.22]	103→107 (86%)	$(\pi^*)_{\text{NPh}_3} \leftarrow (\pi)_{\text{PhNPh}_2}$
<b>4b</b>	604 [8.4]	573 [0.33]	141→142 (98%)	<b>A:</b> $(\pi^*)_{\text{TCBD}} \leftarrow (\pi)_{\text{PhNPh}_2}$
	≈ 505 [sh, 4.9]	545 [0.05]	141→143 (98%)	<b>B:</b> $(\pi^*)_{\text{TCBD}} \leftarrow (\pi)_{\text{PhNPh}_2}$
	354 [16.6]	379 [0.60]	141→144 (95%)	$(\pi^*)_{\text{TCBD/NPh}_2} \leftarrow (\pi)_{\text{PhNPh}_2}$
		345 [0.10]	140→143 (86%)	$(\pi^*)_{\text{TCBD/NPh}_2} \leftarrow (\pi)_{\text{NPh/TCBD}}$
	306 [26.2]	332 [0.19]	141→145 (41%)	$(\pi^*)_{\text{TCBD/Ph}_2\text{N}} \leftarrow (\pi)_{\text{PhNPh}_2}$
<b>4c</b>	581 [10.0]	531 [0.23]	179→180 (98%) 179→181 (98%)	<b>E:</b> $(\pi^*)_{\text{TCBD}} \leftarrow (\pi)_{\text{NPh}_3}$
	≈ 495 [sh, 5.5]	507 [0.02]	179→182 (99%)	<b>A:</b> $((\pi^*)_{\text{TCBD}} \leftarrow (\pi)_{\text{NPh}_3})$
	338 [30.4]	369 [0.45]	179→183 (95%) 179→184 (95%)	<b>E:</b> $(\pi^*)_{\text{TCBD/Ph}} \leftarrow (\pi)_{\text{NPh}_3}$
		345 [0.22]	177→180 (41%) 178→181 (41%)	$(\pi^*)_{\text{TCBD}} \leftarrow (\pi)_{\text{NPh/TCBD}}$
		342 [0.09]	177→182 (26%) 178→181 (25%)	<b>E:</b> $(\pi^*)_{\text{TCBD}} \leftarrow (\pi)_{\text{NPh/TCBD}}$
		304 [0.03]	179→186 (62%) 179→185 (20%)	<b>A:</b> $(\pi^*)_{\text{TCBD/Ph}} \leftarrow (\pi)_{\text{NPh}_3}$ <sup>f</sup>
	305 [36.1]	300 [0.11]	174→181 (38%) 175→182 (39%)	$(\pi^*)_{\text{TCBD}} \leftarrow (\pi)_{\text{NPh}_3}$
		293 [0.09]	176→182 (72%)	$(\pi^*)_{\text{TCBD}} \leftarrow (\pi)_{\text{NPh}_3}$

<sup>a</sup> The calculated (vertical) excited states are <sup>1</sup>A. <sup>b</sup> Experimental absorption (nm) found for the corresponding complex in DCM (or THF for **4a-c**) and extinction coefficients ( $\epsilon$ ) in  $10^3 \text{ M}^{-1} \cdot \text{cm}^{-1}$ . <sup>c</sup> Vertical energy in nm. <sup>d</sup> Computed oscillator strength. <sup>e</sup> See ESI for the plot of the corresponding MOs. <sup>f</sup> Tentative assignment.

The match with experiment is poorer for the organometallic derivatives **5** and **6**. The presence of several *d*-type MOs in the HOMO region (see Figure 6 and Figure S12, ESI) multiplies the number of possible transitions of low energy. Indeed, the four HOMOs of **5** are heavily weighted on the ferrocene groups with some amino lone pair admixture (Figure 6). For **6**, the HOMO is localized on the triphenylamino fragment while the HOMO-1 is strongly localized on the Fc fragment. As a result, contrary to what was computed for the organic derivatives (*vide supra*), the fragment R<sub>2</sub> (Chart 2) is now as electron-releasing as R<sub>1</sub>. Thus, the first

absorption band in **5** and **6** corresponds to a weakly-allowed Fc → TCBD MLCT transition, with a moderate oscillator strength, whereas the next-lowest-energy band for **6** corresponds to the fully allowed and much more intense NPh<sub>3</sub>→TCBD CT transition (Table 5). In a similar way to what was observed for the **3a-c** family, moving from the mono-TCBD derivative **6** to the tri-branched derivative **5** results in additional CT transitions stemming from the threefold symmetry of the latter compound (Figure 6). Overall, the shape of their absorption spectra remains the same, except for some broadening of the first band and a slight red shift of the two first absorption bands in the latter reflecting the decrease in HOMO-LUMO gap between these compounds due to the increasing number of Fc moieties. According to the computations, the electronic coupling between the excitations composing the first MLCT band appears much weaker (< 0.01 eV) in **5**. Due to some intimate mixing of the amino lone pair and ferrocenyl *d* orbitals in the HOMO (**5**) to HOMO-1 (**5-6**), both the first and second absorption bands have a strong MLCT character, with the first band formally corresponding to a pure MLCT band, as evidenced by the difference density plots for these compounds (ESI, Figures S18-S19). Furthermore, consistent with experiment, we confirmed computationally that changing the surrounding medium for **5** (THF vs. CH<sub>2</sub>Cl<sub>2</sub>) hardly affects its electronic spectrum (ESI, Figure S20).

**Table 5.** Experimental vs. computed <sup>a</sup> (mPW1PW91/LANL2DZ/PCM) values in THF. Wavelength (nm) and composition of the first relevant singlet excited states (wavelength [oscillator strength], transition percentage, assignment).

Cmpd	Experimental	Calculated <sup>c</sup>	Composition	Major
	$\lambda_{\max}^b$	$\lambda_{\max} [f^d]$		Assignment <sup>e</sup>
<b>5</b>	608	664 [≈0.02]	303→306 (20%) 303→327 (19%) 303→308 (15%) 303→310 (12%)	( $\pi^*$ ) <sub>NPh<sub>3</sub></sub> ←N+( <i>d</i> ) <sub>Fc</sub>
		661 [≈0.02]	302→309 (22%) 302→326 (19%) 302→306 (14%) 302→308 (13%)	( $\pi^*$ ) <sub>TCBD</sub> ←( <i>d</i> ) <sub>Fc</sub>
		660 [≈0.02]	304→328 (20%) 304→307 (18%) 304→308 (18%) 304→310 (18%)	( $\pi^*$ ) <sub>TCBD</sub> ←( <i>d</i> ) <sub>Fc</sub>
	475	529 [0.36]	305→306 (67%)	( $\pi^*$ ) <sub>TCBD</sub> ←( <i>d</i> ) <sub>Fc</sub>
		528 [0.11]	305→307 (34%)	( $\pi^*$ ) <sub>TCBD</sub> ←( <i>d</i> ) <sub>Fc</sub>
		525 [0.14]	305→306 (18%)	( $\pi^*$ ) <sub>TCBD</sub> ←( <i>d</i> ) <sub>Fc</sub>
		524 [0.32]	305→307 (52%)	( $\pi^*$ ) <sub>TCBD</sub> ←( <i>d</i> ) <sub>Fc</sub>
	350	416 [0.25]	305→309 (87%)	( $\pi^*$ ) <sub>TCBD</sub> ←( <i>d</i> ) <sub>Fc</sub>
		411 [0.31]	305→310 (87%)	( $\pi^*$ ) <sub>TCBD</sub> ←( <i>d</i> ) <sub>Fc</sub>
	<b>6</b>	/	649 [≈0.02]	144→146 (30%) 144→147 (26%) 144→155 (23%)
/		539 [0.30]	145→146 (96%)	( $\pi^*$ ) <sub>TCBD</sub> ←NPh <sub>3</sub>
/		449 [0.51]	145→147 (96%)	( $\pi^*$ ) <sub>TCBD</sub> ←NPh <sub>3</sub>
/		367 [0.10]	142→146 (80%)	( $\pi^*$ ) <sub>TCBD</sub> ←( <i>d</i> ) <sub>xx</sub>
/		308 [0.16]	135→146 (51%)	( $\pi^*$ ) <sub>TCBD</sub> ←NPh <sub>2</sub>
/		285 [0.16]	145→149 (58%)	NPh <sub>3</sub> ←NPh <sub>3</sub>

<sup>a</sup> The calculated (vertical) excited states are <sup>1</sup>A. <sup>b</sup> Experimental wavelength (nm). <sup>c</sup> Vertical energy in nm. <sup>d</sup> Computed oscillator strength. <sup>e</sup> See ESI for the plot of the corresponding MOs.

## Discussion

The nine new TCBD derivatives (**1-5**) that were isolated and studied in this work are two-photon absorbers in the near-IR range (875-1300 nm). DFT calculations on these systems, while confirming previous results independently obtained for some of them,<sup>1, 13</sup> provide a qualitative energy ordering of their excited states. This permits in depth analysis of their nonlinear absorption properties and comparison with literature reports on related compounds such as **A<sub>x</sub>** (X = H, NPh<sub>2</sub>)<sup>24</sup> and **10a-c** (Chart 3).<sup>47</sup> DFT computations also indicate that for all the new compounds investigated, except **4a-c**, a manifold of closely-lying excited states is present at low energy, invalidating the use of essential state models to fully rationalize their 2PA properties. We will thus start the discussion with **4a-c**.

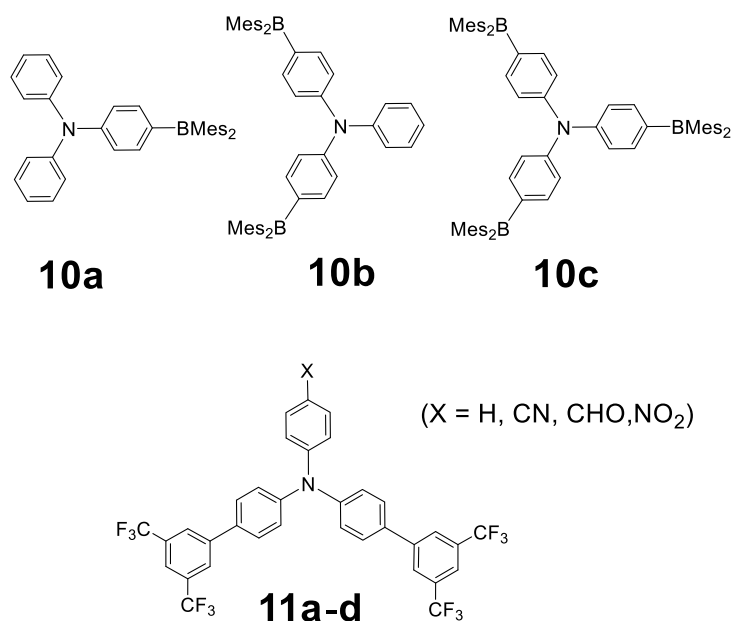


**Chart 3.** Selected two-photon absorbers related to **3a-c** and **4a-c**.

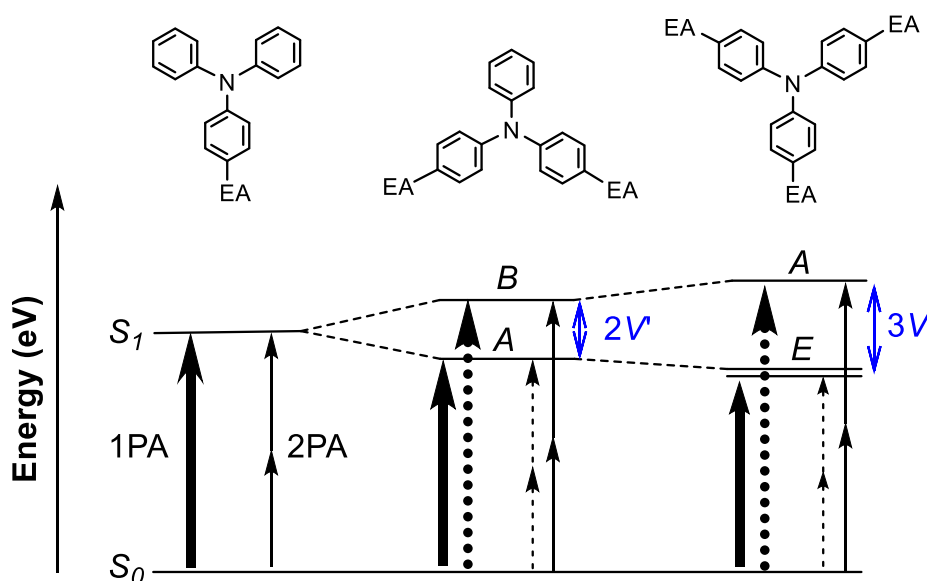


**Figure 7.** Change in allowed (plain arrows)/forbidden (dashed arrows) 1PA and 2PA transitions in the essential state models upon increasing branching in triphenylamine-based derivatives (EA = electron-attracting group).

## 2PA properties of 4a-c

In this series, compound **4a** is dipolar while **4c** is the corresponding octupolar homologue. From the essential state(s) (excitonic) models for such compounds (Figure 7),<sup>35, 56</sup> moving from **4a** to **4c** should result in at least a threefold increase in the 2PA band intensity, but a further improvement in the 2PA response could also ensue from (positive) excitonic coupling between the various branches through the central core, as observed with **10a-c**.<sup>47</sup> The existence of a significant coupling between branches is usually revealed by the splitting of the first 1PA and 2PA bands and by a red shift of the main 2PA vs. the 1PA band when the latter is plotted against twice its wavelength.

It is noteworthy that, contrary to observations with the 1PA spectra of **10a-c**, a progressive blue shift of the first allowed 1PA band is observed when going from **4a** to **4c**. This hypsochromic shift, which is predicted by the calculations, most likely reflects the decrease (saturation) of the electron-donating strength of the central amino atom with the increasing number of electron-accepting branches. As a consequence, the *A* state at higher-energy, resulting from the splitting of the first CT state in **4a** when the number of branches increases, is more blue-shifted than for a compound with a comparable electronic/excitonic coupling in which such a “saturation” of the electron-releasing group does not take place. This saturation effect might also explain the weaker coupling found for **4c** compared to **10c**. Another explanation for the decreased coupling could be the more pronounced conformational flexibility of the TCBD end groups in **4a-c**, leading to more severe disruption of the  $\pi$  manifold in solution at ambient temperatures than for **10a-c**.

The lowest-energy 2PA bands detected for **4a-c** (ESI, Figure S24) are broader than those for **10a-c**. For each compound, we nevertheless noticed a fair spectral match with the main 1PA band when it is plotted at half wavelength, suggesting that 2PA takes place into the 1PA-allowed *E*-state (Figure 8).<sup>d</sup> This state is in principle 2PA-forbidden and a larger 2PA cross-section should be observed for 2PA into the corresponding 1PA-forbidden *A* state in **4c**, at higher energy. This state is predicted to lie 0.11 eV higher in energy by DFT calculations (corresponding to a coupling *V* of ca. 300 cm<sup>-1</sup>). However, no other maxima for a second 2PA peak can be detected in this frequency range, suggesting that these two 2PA transitions overlap to give a single broad 2PA band. In line with such a hypothesis, the cross-section of this first 2PA band increases from 30 GM in **4a** to 100 GM in **4c**, as expected for three weakly coupled dipoles ( $V \leq 0.05$  eV  $\approx$  400 cm<sup>-1</sup>) for which the octupolar system behaves approximately as the sum of the individual arms.<sup>e,47</sup>

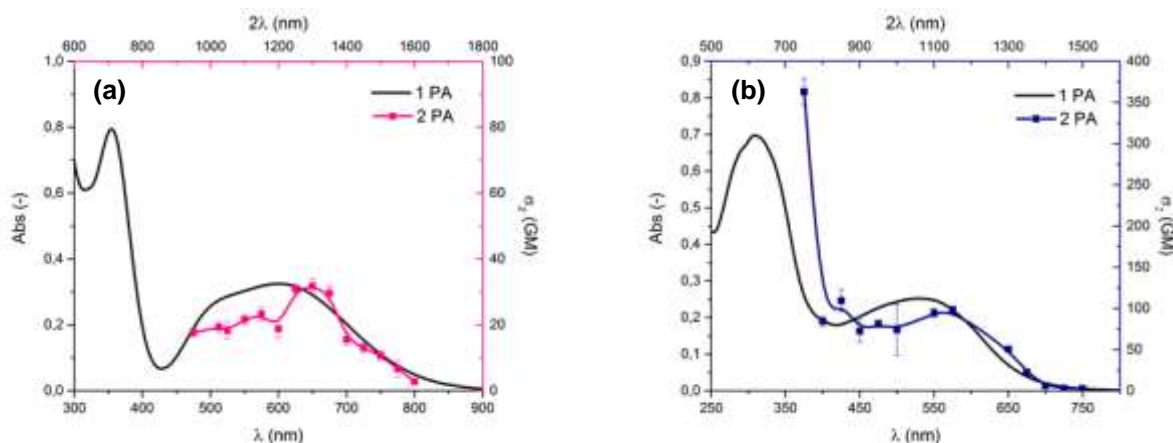


**Figure 8.** Overlay of the 1PA and 2PA spectra for **4a** in CH<sub>2</sub>Cl<sub>2</sub> (a) and **4c** (b) in THF at 25 °C. The 1PA spectra are plotted vs. twice the wavelength ( $2\lambda$ ).

<sup>d</sup> Partial relaxation of the selection rules relative to an ideal *D*<sub>3</sub> (octupolar) structure will populate the forbidden *E* state by 2PA in the trisubstituted derivatives. This phenomenon might be attributed to the flexible nature of these molecules, which can adopt conformations with no strictly octupolar geometries in solution.

<sup>e</sup> We also envisioned the possibility that the second 2PA peak is outside our observation window, in a spectral region with 1PA absorption, and that only the partly forbidden 2PA transition was observed. However, this requires a splitting of ca. 0.5 eV between the first two *A* and *E* excited states, which is one order of magnitude larger than the computational estimates and not consistent with the enhancement observed in the first 2PA band, when computed from the equations derived from the essential states model.

## 2PA properties of 3a-c

A similar situation should exist for the **3a-c** series, except that two 2PA bands are detected for **3a** (Figure 9). In line with DFT computations (Table 5), the latter correspond to population of the two different excited states (CT1 and CT1') which give rise to the first 1PA band. In the branched compounds **3b** and **3c**, each of these states is split into two new states. According to DFT calculations, their splitting is larger in **3a-c** than in **4a-c** but remains below their mean energetic separation (Figure 6). Thus, if the 2PA transitions to these sub-states are not spectrally resolved in **3b** and **3c**, the first 2PA band should correspond to the population of the CT1 states and the second band to that of the CT2 states, and this should result in a roughly threefold improvement in the cross-section of each 2PA band in **3c** compared to those in **3a**, as seen with **4a-c**. However, this is not what is observed; across the series **3a-c**, the first 2PA band does not even double in intensity (it increases from 50 to 80 GM), and a *ca.* five-fold increase is seen with the second 2PA band (from 55 to 275 GM). This departure from predictions of the essential states (excitonic) model in the case of **3a-c** is perhaps the result of its poor applicability given the number of closely-lying excited states at low energy.<sup>6,47</sup> We note that the cross-sections found for **3b** and **4b** in the present studies are of comparable magnitudes to those found from Z-scan studies for the first 2PA transitions (also 1PA-allowed) of non-symmetric triaryl amines such as **11a-d** (Chart 3).<sup>57</sup>

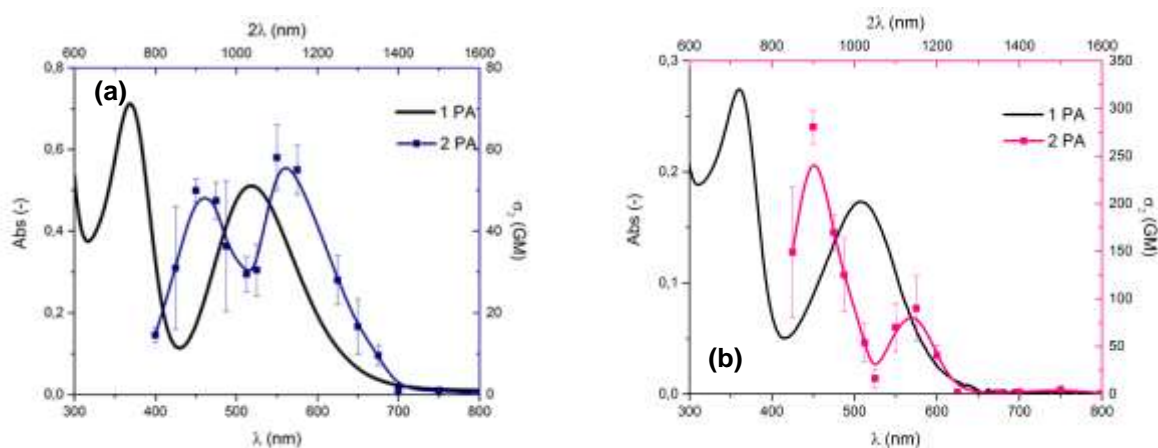


**Figure 9.** Overlay of 1PA and 2PA spectra for **3a** (a) and **3c** (b) in CH<sub>2</sub>Cl<sub>2</sub> at 25 °C. The 1PA spectra are plotted vs. twice the wavelength (2λ).

## 2PA properties of 1, 2 and 5

For the “linear” organic derivatives **1** and **2**, a fair match is observed between the 2PA band and the rescaled lowest energy 1PA band that results from two overlapping transitions (CT1 and CT2), so unambiguous identification of the excited state populated by the first 2PA transition is not possible for these compounds. With the organometallic derivative **5**, the most intense 2PA peak detected for this tri-branched compound overlaps with the second lowest-energy peak of the rescaled 1PA spectrum (Figure 4b). According to the DFT calculations, this second band corresponds to Ph<sub>3</sub>N → TCBD CT transitions, most likely to the *E* subset of states. Likewise, the next two lower-energy 2PA peaks are tentatively attributed to a set of three arm-centered MLCT states, which are only weakly coupled according to DFT. Whether these two peaks correspond to population of the *A* and *E* subsets of these three MLCT states or to the unresolved population of this set and of another set of three 1PA-forbidden <sup>1</sup>MLCT states calculated at slightly lower energies cannot be ascertained as yet.

<sup>f</sup> Another explanation could be that the actual coupling between branches is larger than that given by the computations in **3c** (in **3b**). As a result, the lowest-energy 2PA band would correspond to population of the *E*-CT1 state only (*A*-CT1 state in **3b**), while the next-lowest energy 2PA peak would correspond to two overlapping 2PA transitions to the *A*-CT1 and *E*-CT1' states (*B*-CT1 and *A*-CT1' states in **3b**), while the 2PA transition to the *A*-CT1' state (*B*-CT1' state in **3b**) would not be detected because it is shifted outside the Z-scan observation window. Such a hypothesis would correspond better with the predictions based on the excitonic model of the change in 2PA intensities along the **3a-c** series and would rationalize the detection of three 2PA peaks for **3b**.

## Substituent effects ( $R_1$ , $R_2$ ) and branching

Now that most of the 2PA peaks detected at lower energies have been (tentatively) assigned, we can discuss the data obtained. We showed that the largest 2PA in the near-IR range usually corresponds to  $\text{Ph}_3\text{N} \rightarrow \text{TCBD}$  CT transitions (*i.e.* CT1 in Chart 2). Among the mono-TCBD compounds, those affording the largest 2PA cross-sections at lowest energy are the disubstituted TCBD derivatives ( $R_1$  and  $R_2 \neq \text{H}$ ) with the 2PA cross-sections scaling with electron-releasing power of the substituents  $R_1$  and  $R_2$  in the ordering:  $4\mathbf{a} < 3\mathbf{a} \approx \mathbf{1} < \mathbf{2} \approx \mathbf{A}_\text{H} < \mathbf{A}_{\text{NPh}_2}$ , emphasizing the importance of multipolar structures over those purely dipolar in nature,<sup>35, 46</sup> such as  $4\mathbf{a}$ .<sup>g,58</sup>

We also found that a modest but positive synergy can result from branching around the nitrogen atom in diphenylanilino-substituted TCBD derivatives, with cross-sections values in the range of those reported for other push-pull triphenylamino derivatives such as  $11\mathbf{a-d}$ . Furthermore, for branched derivatives, especially when the excitonic/electronic coupling is positive and strong, the most active 2PA A state is usually shifted to higher energies, closer to the edge of the 1PA-transparency window of the compound, a shift increased by the so-called “saturation” effect observed for TCBD substituents. In this respect, disubstituting the TCBD moiety by another electron-releasing substituent does reduce the electron-accepting strength of this unit and therefore contributes to limiting the blue shift of the A state induced by branching. As a result,  $3\mathbf{c}$  constitutes a significantly more active two-photon absorber than  $4\mathbf{c}$ , at a slightly lower wavelength (900 vs. 1150 nm), but still in the near-IR range. Finally, substituting the TCBD unit with organometallic electron-releasing substituents instead of purely organic ones, as in  $5$ , confers some MLCT character to the CT1 states which also favors their 2PA cross-section.<sup>37-39</sup> This structural change also made the CT2 states ( $\text{Fc} \rightarrow \text{TCBD}$ ) more stable than the CT1 ones ( $\text{Ph}_3\text{N} \rightarrow \text{TCBD}$ ) and contributed to a shift in the latter to higher energies. Nevertheless, the cross-sections are improved in  $5$  relatively to those of the corresponding 2PA bands in  $3\mathbf{c}$  or  $4\mathbf{c}$ . Remarkably, the 2PA transitions detected at lower energy (into the CT2 states) for  $5$  have significantly lower cross-sections, although they have in principle a much more pronounced metallic character. This might result from weaker electronic coupling between the peripheral CT excitons of these MLCT states or from their comparatively low transition dipole moments.

When the various cross-sections are normalized against the molecular weight or against the number of effective electrons,<sup>59</sup> the resulting figures of merit indicate that the best 2PA absorbers among the new derivatives are  $5$  followed by  $3\mathbf{c}$ , with 2PA performance below that of the known  $\mathbf{A}_{\text{NPh}_2}$ .<sup>24</sup> These results reveal that the increase stated for  $5$  compared to  $3\mathbf{c}$  stems largely from the number of effective electrons introduced by the peripheral ferrocenyl substituents and not only from its more electron-releasing-character or from the presence of polarizable  $d$  MOs. More generally, contrary to what had been found for fluorescence,<sup>29</sup> these results indicate that electron-rich substituents, which give rise to CT states at low energy, are clearly more desirable than none in enhancing the 2PA properties of TCBD derivatives.<sup>24</sup> Given their very weak fluorescence in solution at ambient temperatures, their third-order activity make them better suited for applications such as optical-limiting in the near-IR range,<sup>44, 60, 61</sup> and beam re-shaping in the far IR range, as well as applications not related to their transparency, such as 2PA sensitization for nanolithography or photodynamic therapy.<sup>32</sup> Furthermore, as previously underlined by Shoji and coworkers,<sup>13</sup> organometallic derivatives such as  $5$  might give rise to innovative electro-switchable NLO-active substances.<sup>36</sup>

## Conclusions

Four new compounds ( $1$ ,  $3\mathbf{c}$  and  $4\mathbf{b-c}$ ) featuring TCBD units functionalized by tosylamido and/or 4- $N,N$ -diphenylanilino side-groups have been synthesized and characterized. We have shown that when a single 4-diphenylanilino substituent is appended at the 2-position ( $R_1$ , Chart 2) of the TCBD moiety ( $4\mathbf{a}$ ), a fairly reactive dipolar compound is formed. However, we also show that this dipolar compound can be stabilized either by using a less electron-rich aromatic  $R_1$  group or by appending another  $\pi$ -conjugated substituent at the 3-position ( $R_2$ ) such as a tosylamido ( $1$ ,  $2$ ,  $3\mathbf{a-c}$ ) or ferrocenyl ( $5$ ) group.

The 1PA and 2PA properties of compounds  $1-5$  were subsequently investigated, revealing that all of them are two-photon absorbers in the near-IR range (875-1300 nm). Thus, while derivative  $1$  is a poorer two-photon absorber than its known 4- $N,N$ -diphenylanilino analogue ( $\mathbf{A}_\text{H}$ ), we have shown herein that among the tosylamido derivatives, the 2PA activity can notably be improved by appending more electron-rich aromatic groups to the remaining position of the TCBD group, a change which also induces a red-shift in the 2PA maxima. When the aromatic group was replaced by a 4- $N,N$ -diarylanilino substituent, the possibility of branching at the central nitrogen opens options for further increasing the 2PA activity. Accordingly, the di- and tri-branched derivatives  $3\mathbf{b}$  and  $3\mathbf{c}$  surpass  $\mathbf{A}_\text{H}$  in terms of 2PA cross-section, the latter ( $3\mathbf{c}$ ) showing the best  $\sigma_2^{\text{max}}$  value among the new organic derivatives tested. With the aid of DFT calculations, which provided a qualitative understanding of the nature of the first singlet excited states of  $1-5$ , a comparison with the analogous family without the tosylamido group(s)  $4\mathbf{a-c}$  was made. This revealed the

<sup>g</sup> The tosylamido group is a far less effective electron-releasing group than the 4- $N,N$ -diphenylanilino group.<sup>58</sup>



positive role exerted by the tosylamido substituent(s) on the 2PA activity in spite of the fact that these substituents reduce the electron-accepting character of the TCBD units in **3a-c** compared to those in **4a-c**. In this respect, the present investigation points to the importance of the multipolar character of each branch in these compounds. Finally, a further enhancement of the 2PA cross-section was achieved by proceeding to the organometallic derivative **5**, in other words, by replacing the tosylamido endgroups by an even more electron-releasing substituent. In line with the good 2PA performance previously stated for **A<sub>NPh2</sub>**, this further underlines the positive effect of having electron-releasing substituents at both positions on the TCBD unit for boosting the 2PA cross-sections of such compounds while illustrating further the positive impact of organometallic substituents on the third-order NLO properties of these multipolar molecules.

## Experimental Section

**General.** All reactions and work-up procedures of air-sensitive compounds were carried out under dry, high-purity argon or nitrogen, using standard Schlenk techniques.<sup>62</sup> Solvents/reagents were dried and distilled as follows: Et<sub>2</sub>O, hexane and reagent grade THF (sodium-benzophenone), CH<sub>2</sub>Cl<sub>2</sub> (CaH<sub>2</sub>), diisopropylamine and triethylamine (KOH), and DMF (activated 3 Å molecular sieves). Flash column chromatography was performed using silica (Acros 60 Å, 40-60 mesh). Melting points were taken in air using a melting point apparatus. NMR spectra were acquired at 298 K on 400 and/or 500 MHz FT NMR spectrometers. UV-Vis-NIR spectra were recorded using a 1 cm quartz cell on a Cary 5 spectrometer, and are reported as  $\lambda_{\max}$  (nm) [ $\epsilon$  (10<sup>3</sup> M<sup>-1</sup>.cm<sup>-1</sup>)]. High-resolution mass spectra (EI and ESI) were obtained at the Centre Regional de Mesures Physiques de l'Ouest (CRMPO, Rennes) or at Wroclaw University of Science and Technology (WUST). The synthesis of the alkyne precursors **6** and **7c** and of **5<sup>13</sup>** are described in the ESI. The alkynes **8b-c**<sup>42,63</sup> and **9<sup>43</sup>** are known compounds. Other chemicals were purchased from a commercial source and used as received.

### Synthesis of **1**, **3c** and **4b-c**

**Typical experimental procedure for the formation of the TCBD compounds **1**, **3c**, **4b-c**.** A solution of ynamide (1.0 equiv) and tetracyanoethene (1.0, 2.0 or 3.0 equiv) in CH<sub>2</sub>Cl<sub>2</sub> (0.1 M) was stirred at room temperature for 12 h. For **1** and **3c**, the solvent was evaporated and the residue was subjected to chromatography on silica gel to afford the TCBD moieties. Products **4b-c** were recrystallized from crude reaction mixtures.

**Synthesis of compound **1**.** The reaction mixture was purified by column chromatography (petroleum ether/Et<sub>2</sub>O [4:1] to [1:1]) to give the title compound (60 mg, 88%) as an orange solid. Crystals were grown by slow diffusion of cyclohexane into a solution of this compound in CH<sub>2</sub>Cl<sub>2</sub>. **MP:** decomposition above 80 °C. **R<sub>f</sub>:** 0.55 (petroleum ether/EtOAc [1:1]). **<sup>1</sup>H NMR** (400 MHz, CDCl<sub>3</sub>):  $\delta$  = 7.90 (1H, d, *J* 8.1 Hz), 7.84 – 7.79 (2H, m), 7.77 (2H, d, *J* 8.4 Hz), 7.63 (1H, dd, *J* 1.8 and 8.1 Hz), 7.50 – 7.38 (5H, m), 3.46 (3H, s), 2.50 (3H, s), 2.17 – 1.95 (4H, m), 1.16 – 1.08 (4H, m), 0.68 (6H, t, *J* 7.3 Hz), 0.65 – 0.51 (4H, m). **<sup>13</sup>C{<sup>1</sup>H} NMR** (100 MHz, CDCl<sub>3</sub>):  $\delta$  = 165.5, 164.5, 152.6, 152.4, 148.3, 147.5, 139.1, 132.5, 131.0, 129.8, 128.4, 127.6, 125.7, 123.4, 121.5, 121.0, 112.6, 112.4, 110.9, 110.7, 87.5, 80.4, 55.9, 41.2, 40.1, 26.0, 23.1, 22.0, 13.9. **HRMS:** calculated for C<sub>37</sub>H<sub>36</sub>N<sub>5</sub>O<sub>2</sub>S [M+H]<sup>+</sup> 614.259, found 614.258. **Crystal data** (CCDC 2081542): C<sub>75</sub>H<sub>76</sub>N<sub>12</sub>O<sub>4</sub>S<sub>2</sub>, *M* = 1273.59 g.mol<sup>-1</sup>, *T* = 150 K, triclinic, space group =  $P\bar{1}$ , *a* = 12.2334(10) Å, *b* = 16.0882(15) Å, *c* = 18.7919(16) Å,  $\alpha$  = 107.984(3)°,  $\beta$  = 97.849(3)°,  $\gamma$  = 90.566(3)°, *V* = 3479.5(5) Å<sup>3</sup>, *Z* = 2.

**Synthesis of compound **3c**.** The reaction mixture was purified by column chromatography (cyclohexane/CH<sub>2</sub>Cl<sub>2</sub> [1:1] to [0:1]) to give the title compound (77 mg, 82%) as a dark purple solid. Crystals were grown by slow diffusion of cyclohexane into a solution of this compound in CH<sub>2</sub>Cl<sub>2</sub>. **<sup>1</sup>H NMR** (400 MHz, CD<sub>2</sub>Cl<sub>2</sub>):  $\delta$  = 7.97 (d, *J* = 8.1 Hz, 6H), 7.52 (d, *J* = 8.1 Hz, 6H), 7.39 (t, *J* = 7.3 Hz, 3H), 7.33 (t, *J* = 7.4 Hz, 6H), 7.28 – 7.13 (m, 18H), 4.86 (s, 6H), 2.52 (s, 9H). **<sup>13</sup>C{<sup>1</sup>H} NMR** (100 MHz, CD<sub>2</sub>Cl<sub>2</sub>):  $\delta$  = 164.90, 158.7, 149.6, 147.8, 132.9, 131.6, 131.3, 131.0, 129.8, 129.5, 129.3, 128.4, 125.9, 124.9, 111.8, 111.7, 111.6, 111.2, 91.5, 81.6, 52.7, 21.7. **HRMS:** calculated for C<sub>84</sub>H<sub>54</sub>N<sub>16</sub>O<sub>6</sub>S<sub>3</sub> [M]<sup>+</sup> 1478.357, found 1478.358. **Crystal data** (CCDC 2080796): C<sub>84</sub>H<sub>54</sub>N<sub>16</sub>O<sub>6</sub>S<sub>3</sub> *M* = 1479.61 g.mol<sup>-1</sup>, *T* = 150 K, trigonal, space group =  $R\bar{3}$ , *a* = 21.023(2) Å, *b* = 21.023(2) Å, *c* = 30.595(3) Å,  $\alpha$  = 90°,  $\beta$  = 90°,  $\gamma$  = 120°, *V* = 11710(3) Å<sup>3</sup>, *Z* = 6.

**Synthesis of compound **4b**.** This compound was precipitated from the reaction mixture following addition of pentane to give the title compound (72 mg, 67%) as a dark blue solid. Crystals were grown by slow diffusion of cyclohexane into a solution of this compound in CH<sub>2</sub>Cl<sub>2</sub>. **<sup>1</sup>H NMR** (400 MHz, acetone-*d*<sub>6</sub>):  $\delta$  = 8.57 (2H, s), 7.72 (4H, d, *J* 8.9 Hz), 7.53 – 7.44 (2H, m), 7.38 – 7.25 (7H, m). **<sup>13</sup>C{<sup>1</sup>H} NMR** (100 MHz, acetone-*d*<sub>6</sub>):  $\delta$  = 162.3, 155.4, 151.8, 145.8, 132.2, 130.7, 127.4, 126.9, 126.1, 123.9, 113.0, 112.9, 112.1, 110.0, 97.3, 89.2. **HRMS:** calculated for C<sub>34</sub>H<sub>15</sub>N<sub>9</sub> [M]<sup>-</sup> 549.1456, found 549.1457. **UV-Vis** (THF):  $\lambda_{\max}$  = 552 [8.4], 490 [sh],

7.3], 340 [sh, 20.3], 308 [25.7]. **Crystal data** (CCDC 992932): C<sub>34</sub>H<sub>16</sub>N<sub>9</sub>, *M* = 549.55 g.mol<sup>-1</sup>, *T* = 140 K, monoclinic, space group = *P*2<sub>1</sub>/*a*, *a* = 10.7358(5) Å, *b* = 9.7979(4) Å, *c* = 13.1395(4) Å,  $\alpha$  = 90.00°,  $\beta$  = 93.928(3)°,  $\gamma$  = 90.00°, *V* = 1378.87(10) Å<sup>3</sup>, *Z* = 2.

**Synthesis of compound 4c.** This compound was precipitated from reaction mixture following addition of pentane to give the title compound (63 mg, 58%) as a dark blue solid. <sup>1</sup>H NMR (400 MHz, acetone-*d*<sub>6</sub>):  $\delta$  = 8.57 (3H, s), 7.76 (6H, d, *J* 8.8 Hz), 7.45 (6H, d, *J* 8.8 Hz). <sup>13</sup>C{<sup>1</sup>H} NMR (100 MHz, acetone-*d*<sub>6</sub>):  $\delta$  = 163.3, 155.8, 151.8, 133.4, 128.6, 126.7, 113.9, 113.8, 112.9, 111.0, 98.3, 92.0. **UV-Vis** (THF):  $\lambda_{\text{max}}$  = 528 [12.6], 308 [34.9]. **HRMS**: calculated for C<sub>42</sub>H<sub>15</sub>N<sub>13</sub> [M]<sup>+</sup>: 701.1579, found 701.1580.

## Z-scan studies on 1-5

Measurements of the third-order nonlinear optical properties were carried out using the Z-scan technique over a wide range of wavelengths and were performed by employing a Quantronix Integra Ti:Sapphire regenerative amplifier (output wavelength 800 nm) pumping a Quantronix-Palitra-FS optical parametric amplifier which delivered wavelength tuneable pulses with a duration of about 130 fs at a repetition rate of 1 kHz. The output beam was selected with a polarization separator, passed through a suitable colour glass filter to reject unwanted wavelengths and attenuated using neutral density filters. The peak incident intensities of the beam were of the order of 100 GW cm<sup>-2</sup>. Results obtained for samples in THF or CH<sub>2</sub>Cl<sub>2</sub> solutions (of ca. 0.5 w/w% concentration) placed in 1 mm stoppered Starna glass cells were calibrated against Z-scan measurements on a fused silica plate and compared with the measurements on an identical glass cell filled with the pure solvent.<sup>49</sup> The obtained data were analysed with the help of a custom fitting program that used equations derived by Sheik-Bahae *et al.*<sup>64</sup>

## DFT calculations

Geometry optimization of all molecules (**C1-C7**, **A<sub>H</sub>**) were carried out at the density functional theory (DFT) level of theory using the Gaussian 09 program package.<sup>65</sup> Real molecules (**2-5**) were considered for optimization geometry calculations (**C2-C5**), except **1** in which the butyl chains were replaced by methyl groups to reduce computational efforts (**C1**). In addition, **C6** representing a single branch of **C5**, and **A<sub>H</sub>** were also computed for comparison purpose. Optimization was conducted in the gas phase (no solvent effect) without any symmetry constraint for all compounds, except for the two organometallic complexes (**C5** and **C6**), where THF (Polarizable Continuum Model (PCM))<sup>66</sup> was considered because of their more polarizable *d* orbitals. The hybrid functional mPW1PW91 functional (which consists of a modified version of the PW91 exchange functional with PW91 correlation functional and a mixing ratio of exact and DFT exchange of 0.25 to 0.75) was employed<sup>67</sup> in combination with the LANL2DZ basis set for all the atoms.<sup>68</sup> Frequency calculations were carried out for all structures to check the nature of the stationary states and the absence of any imaginary frequency to confirm that the optimized geometries were genuine minima on the potential energy hypersurface. Time-dependent density functional theory (TD-DFT)<sup>69</sup> calculations were performed at the same level of theory using the previously optimized geometries. The UV-Vis spectra were simulated from the computed TD-DFT transition energies and their oscillator strength by using SWizard.<sup>70</sup> GaussView<sup>71</sup> was employed to generate molecular orbital and electron density difference plots.

## Author Contributions

Conceptualization, Y.T. and F.P.; Formal Analysis, M.Z., T.R., L.T., M.C. and G.M.; Funding Acquisition, Y.T. and F.P.; Investigation, N.R., M. B., C.P., Z.P., M.D. and H.S.; Methodology, O.M.; Project Administration, Y.T. and F.P.; Supervision, Y.T., K.M., J.-F.H., M.G.H. and F.P.; Writing – original draft, N.R., M.B., C.P., Z.P., M.D. and H.S.; Writing – review & editing, Y.T., K.M., M.S., J.-F.H., M.G.H. and F.P.

## Conflicts of interest

There are no conflicts to declare.

## Acknowledgements

This research was supported by grants from Campus France (PHC Polonium Program 2017 N°37629XG), the National Science Centre of Poland (NCN Opus UMO-2019/35/B/ST4/03280 and Harmonia UMO-2016/22/M/ST4/00275, Wroclaw University of Science and Technology), the Erasmus Plus program (M.D. and Z.P.), the CNRS (PICS programs N° 5676 & 7106 and LIA Redochrom), the “Region Bretagne” (N.R., M.B. and C.P.), the Agence Nationale pour la Recherche

(JCJC Fluotet 17-CE07-0038-01) and the Australian Research Council (M.G.H.: DP170100408). Calculations were carried out at the Wroclaw Centre for Networking and Supercomputing and at the local computing center from the ISCR (France). H.S. acknowledges the Algerian PRFU project (2020-2024: Grant No. B00L01UN3501202-00003).

## References

1. M. Betou, N. Kerisit, E. Meledje, Y. R. Leroux, C. Katan, J.-F. Halet, J.-C. Guillemin and Y. Trolez, *Chem. Eur. J.*, 2014, **20**, 9553-9557.
2. T. Shoji, E. Shimomura, M. Maruyama, A. Maruyama, S. Ito, T. Okujima, K. Toyota and N. Morita, *Eur. J. Org. Chem.*, 2013, 7785-7799.
3. R. Misra, P. Gautam and S. M. Mobin, *J. Org. Chem.*, 2013, **78**, 12440-12452.
4. R. Garcia, M. A. Herranz, M. R. Torres, P.-A. Bouit, J. L. Delgado, J. Calbo, P. M. Viruela, E. Ortí and N. Martín, *J. Org. Chem.*, 2012, **77**, 10707-10717.
5. D. Koszelewski, A. Nowak-Król and D. T. Gryko, *Chem. Asian J.*, 2012, **7**, 1887-1894.
6. T. Shoji, J. Higashi, S. Ito, T. Okujima, M. Yasunami and N. Morita, *Chem. Eur. J.*, 2011, **17**, 5116-5129.
7. X. Tang, W. Liu, J. Wu, C.-S. Lee, J. You and P. Wang, *J. Org. Chem.*, 2010, **75**, 7273-7278.
8. S.-I. Kato, M. Kivala, W. B. Schweizer, C. Boudon, J.-P. Gisselbrecht and F. Diederich, *Chem. Eur. J.*, 2009, **15**, 8687-8691.
9. T. Shoji, S. Ito, K. Toyota, M. Yasunami and N. Morita, *Chem. Eur. J.*, 2008, **14**, 8398-8408.
10. Y. Morioka, N. Yoshizawa, J.-I. Nishida and Y. Yamashita, *Chem. Lett.*, 2004, **33**, 1190-1191.
11. T. Mochida and S. Yamazaki, *J. Chem. Soc. Dalton Trans.*, 2002, 3559-3564.
12. X. Wu, J. Wu, Y. Liu and A. K.-Y. Jen, *J. Am. Chem. Soc.*, 1999, **121**, 472-473.
13. T. Shoji, N. Kamata, A. Maruyama, S. Ito and T. Okujima, *Bull. Chem. Soc. Jpn.*, 2015, **88**, 1338-1346.
14. T. Shoji and S. Ito, *Chem. Eur. J.*, 2017, **23**, 16696-16709.
15. J. C. May, I. Biaggio, F. Bures and F. Diederich, *Appl. Phys. Lett.*, 2007, **90**, 251106/251101-251103.
16. J. C. May, J. H. Lim, I. Biaggio, N. P. Moonen, T. Michinobu and F. Diederich, *Opt. Lett.*, 2005, **30**, 3057-3059.
17. T. Michinobu, J. C. May, J. H. Lim, C. Boudon, J.-P. Gisselbrecht, P. Seiler, M. Gross, I. Biaggio and F. Diederich, *Chem. Commun.*, 2005, 737-739.
18. B. Esembeson, M. L. Scimeca, T. Michinobu, F. Diederich and I. Biaggio, *Adv. Mater.*, 2008, **20**, 4584-4587.
19. M. Kivala and F. Diederich, *Acc. Chem. Res.*, 2009, **42**, 235-248.
20. S.-I. Kato and F. Diederich, *Chem. Commun.*, 2010, **46**, 1994-2006.
21. T. Michinobu and F. Diederich, *Angew. Chem. Int. Ed.*, 2018, **57**, 3552-3577.
22. F. Monti, A. Venturini, A. Nenov, F. Tancini, A. D. Finke, F. Diederich and N. Armaroli, *J. Phys. Chem. A*, 2015, **119**, 10677-10683.
23. F. Tancini, F. Monti, K. Howes, A. Belbakra, A. Listorti, W. B. Schweizer, P. Reutenauer, J.-L. Alonso-Gomez, C. Chiorboli, L. M. Urner, J.-P. Gisselbrecht, C. Boudon, N. Armaroli and F. Diederich, *Chem. Eur. J.*, 2014, **20**, 202-216.
24. Z. Pokladek, N. Ripoché, M. Betou, Y. Trolez, O. Mongin, J. Olesiak-Banska, K. Matczyszyn, M. Samoc, M. G. Humphrey, M. Blanchard-Desce and F. Paul, *Chem. Eur. J.*, 2016, **22**, 10155-10167.
25. A. T. Bui, C. Philippe, M. Beau, N. Richy, M. Cordier, T. Roisnel, L. Lemiègre, O. Mongin, F. Paul and Y. Trolez, *Chem. Commun.*, 2020, **56**, 3571-3574.
26. C. Philippe, A. T. Bui, S. Batsongo-Boulingui, Z. Pokladek, K. Matczyszyn, O. Mongin, L. Lemiègre, F. Paul, T. A. Hamlin and Y. Trolez, *Org. Lett.*, 2021, **23**, 2007-2012.
27. J. Xu, X. Liu, J. Lv, M. Zhu, C. Huang, W. Zhou, X. Yin, H. Liu, Y. Li and J. Ye, *Langmuir*, 2008, **24**, 4231-4237.
28. K. A. Winterfeld, G. Lavarda, J. Guilleme, M. Sekita, D. M. Guldi, T. Torres and G. Bottari, *J. Am. Chem. Soc.*, 2017, **139**, 5520-5529.
29. A. H. Dar, V. Gowri, A. Gopal, A. Muthukrishnan, A. Bajaj, S. Sartaliya, A. Selim, M. E. Ali and G. Jayamurugan, *J. Org. Chem.*, 2019, **84**, 8941-8947.
30. M. Betou, R. J. Durand, A. Sallustrau, C. Gousset, E. Le Coz, Y. R. Leroux, L. Toupet, E. Trzop, T. Roisnel and Y. Trolez, *Chem. Asian J.*, 2017, **12**, 1338-1346.
31. R. Bouvier, R. Durand, L. Favereau, M. Srebo-Hooper, V. Dorcet, T. Roisnel, N. Vanthuyne, Y. Vesga, J. Donnelly, F. Hernandez, J. Autschbach, Y. Trolez and J. Crassous, *Chem. Eur. J.*, 2018, **24**, 14484-14494.
32. G. S. He, L.-S. Tan, Q. Zheng and P. N. Prasad, *Chem. Rev.*, 2008, **108**, 1245-1330.
33. M. Pawlicki, H. A. Collins, R. G. Denning and H. L. Anderson, *Angew. Chem. Int. Ed.*, 2009, **48**, 3244-3266.
34. H. M. Kim and B. R. Cho, *Chem. Commun.*, 2009, 153-164.
35. F. Terenziani, C. Katan, E. Badaeva, S. Tretiak and M. Blanchard-Desce, *Adv. Mater.*, 2008, **20**, 4641-4678.
36. G. Grelaud, M. P. Cifuentes, F. Paul and M. G. Humphrey, *J. Organomet. Chem.*, 2014, **751**, 181-200.
37. J. Massue, J. Olesiak-Banska, E. Jeanneau, C. Aronica, K. Matczyszyn, M. Samoc, C. Monnereau and C. Andraud, *Inorg. Chem.*, 2013, **52**, 10705-10707.

38. A. Triadon, G. Grelaud, N. Richey, O. Mongin, G. J. Moxey, I. M. Dixon, X. Yang, G. Wang, A. Barlow, J. Rault-Berthelot, M. P. Cifuentes, M. G. Humphrey and F. Paul, *Organometallics*, 2018, **37**, 2245-2262.
39. E. Garoni, A. Colombo, K. Kamada, C. Dragonetti and D. Roberto, *Inorganics*, 2019, **7**, 67 (61-12).
40. A. Coste, G. Karthikeyan, F. Couty and G. Evano, *Angew. Chem. Int. Ed.*, 2009, **48**, 4381-4385.
41. Y. Zhang, R. P. Hsung, M. R. Tracey, K. C. M. Kurtz and E. L. Vera, *Org. Lett.*, 2004, **6**, 1151-1154.
42. G. Grelaud, M. P. Cifuentes, T. Schwich, G. Argouarch, S. Petrie, R. Stranger, F. Paul and M. G. Humphrey, *Eur. J. Inorg. Chem.*, 2012, 65-75.
43. K. R. J. Thomas and J. T. Lin, *J. Organomet. Chem.*, 2001, **637-639**, 139-144.
44. R. Misra, R. Maragani, B. Pathak, P. Gautam and S. M. Mobin, *RSC Adv.*, 2015, **5**, 71046-71051.
45. S. Amthor, B. Noller and C. Lambert, *Chem. Phys.*, 2005, **316**, 141-152.
46. C. Katan, F. Terenziani, O. Mongin, M. H. V. Werts, L. Porrès, T. Pons, J. Mertz, S. Tretiak and M. Blanchard-Desce, *J. Phys. Chem. A*, 2005, **109**, 3024-3037.
47. N. S. Makarov, S. Mukhopadhyay, K. Yesudas, J.-L. Brédas, J. W. Perry, A. Pron, M. Kivala and K. Müllen, *J. Phys. Chem. A*, 2012, **116**, 3781-3793.
48. Y. S. Sohn, D. N. Hendrickson and H. B. Gray, *J. Am. Chem. Soc.*, 1971, **93**, 3603-3612.
49. M. Samoc, A. Samoc, B. Luther-Davies, M. G. Humphrey and M.-S. Wong, *Opt. Mater.*, 2002, **21**, 485-488.
50. K. D. Belfield, M. V. Bondar, F. E. Hernandez, O. V. Przhonska and S. Yao, *J. Phys. Chem. B*, 2007, **111**, 12723-12729.
51. M. G. Kuzyk, *J. Chem. Phys.*, 2003, **119**, 8327-8334.
52. M. G. Kuzyk, *J. Mater. Chem.*, 2009, **19**, 7444-7465.
53. C. Adamo and D. Jacquemin, *Chem. Soc. Rev.*, 2013, **42**, 845-856.
54. A. Laurent and D. Jacquemin, *J. Quantum Chem.*, 2013, **113**, 2019-2039.
55. M.-S. Liao, Y. Lu and S. Schneider, *J. Comput. Chem.*, 2003, **24**, 623-631.
56. D. Beljonne, W. Wenseleers, E. Zojer, Z. Shuai, H. Vogel, S. J. K. Pond, J. W. Perry, S. R. Marder and J.-L. Brédas, *Adv. Funct. Mater.*, 2002, **12**, 631-641.
57. M. G. Vivas, D. L. Silva, J. Malinge, M. Boujtita, R. Zalesny, W. Bartkowiak, H. Ågren, S. Canuto, L. De Boni, E. Ishow and C. R. Mendonca, *Sci. Rep.*, 2014, **4**, 1-11.
58. C. Hansch, A. Leo and R. W. Taft, *Chem. Rev.*, 1991, **91**, 165-195.
59. R. L. Roberts, T. Schwich, T. C. Corkery, M. P. Cifuentes, K. A. Green, J. D. Farmer, P. J. Low, T. B. Marder, M. Samoc and M. G. Humphrey, *Adv. Mater.*, 2009, **21**, 2318-2322.
60. Q. Bellier, N. S. Makarov, P.-A. Bouit, S. Rigaut, K. Kamada, P. Feneyrou, G. Berginc, O. Maury, J. W. Perry and C. Andraud, *Phys. Chem. Chem. Phys.*, 2012, **14**, 15299-15307.
61. T. Jadhav, R. Maragani, R. Misra, V. Sreeramulu, D. N. Rao and S. M. Mobin, *Dalton Trans.*, 2013, **42**, 4340-4342.
62. D. F. Shriver and M. A. Drezdson, *The Manipulation of Air-Sensitive Compounds*, Wiley, New York, 1986.
63. M. Mba, M. D'Acunzo, P. Salice, T. Carofiglio, M. Maggini, S. Caramori, A. Campana, A. Aliprandi, R. Argazzi, S. Carli and C. A. Bigozzi, *J. Phys. Chem. C*, 2013, **117**, 19885-19896.
64. M. Sheik-Bahae, A. A. Said, T. Wei, D. J. Hagan and E. W. Van Stryland, *IEEE J. Quant. Electr.*, 1990, **26**, 760-769.
65. M. J. Frisch, G. W. Trucks, H. B. Schlegel, G. E. Scuseria, M. A. Robb, J. R. Cheeseman, G. Scalmani, V. Barone, G. A. Petersson, H. Nakatsuji, X. Li, M. Caricato, A. Marenich, J. Bloino, B. G. Janesko, R. Gomperts, B. Mennucci, H. P. Hratchian, J. V. Ortiz, A. F. Izmaylov, J. L. Sonnenberg, D. Williams-Young, F. Ding, F. Lipparini, F. Egidi, J. Goings, B. Peng, A. Petrone, T. Henderson, D. Ranasinghe, V. G. Zakrzewski, J. Gao, N. Rega, G. Zheng, W. Liang, M. Hada, M. Ehara, K. Toyota, R. Fukuda, J. Hasegawa, M. Ishida, T. Nakajima, Y. Honda, O. Kitao, H. Nakai, T. Vreven, K. Throssell, J. A. Montgomery, Jr., J. E. Peralta, F. Ogliaro, M. Bearpark, J. J. Heyd, E. Brothers, K. N. Kudin, V. N. Staroverov, T. Keith, R. Kobayashi, J. Normand, K. Raghavachari, A. Rendell, J. C. Burant, S. S. Iyengar, J. Tomasi, M. Cossi, J. M. Millam, M. Klene, C. Adamo, R. Cammi, J. W. Ochterski, R. L. Martin, K. Morokuma, O. Farkas, J. B. Foresman and D. J. Fox, ed. I. Gaussian Program version 09, Revision A.03, Wallingford CT, 2016.
66. J. Tomasi, B. Mennucci and R. Cammi, *Chem. Rev.*, 2005, **105**, 2999-3093.
67. C. Adamo and V. Barone, *J. Chem. Phys.*, 1998, **108**, 664-675.
68. T. H. Dunning, Jr. and P. J. Hay, in *Modern Theoretical Chemistry*, Plenum, New York 1977 (vol. 3), pp. 1-28.
69. E. Runge and E. K. U. Gross, *Phys. Rev. Lett.*, 1984, **52**, 997-1000.
70. S. I. Gorelsky, SWizard program, Revision 4.5., University of Ottawa, Canada, 2013.
71. R. Dennington, T. Keith and J. Millam, Semichem Inc., Shawnee Mission, KS2003.